

Ligand Macrocycle Structural Effects on Copper–Dioxygen Reactivity

Bernice M. T. Lam,[†] Jason A. Halfen,[†] Victor G. Young, Jr.,[†] John R. Hagadorn,[†] Patrick L. Holland,[†] Agustí Lledós,[‡] Lourdes Cucurull-Sánchez,[‡] Juan J. Novoa,[§] Santiago Alvarez,^{*,||} and William B. Tolman^{*,†}

Department of Chemistry and Center for Metals in Biocatalysis, University of Minnesota, 207 Pleasant Street SE, Minneapolis, Minnesota 55455, Departament de Química, Universitat Autònoma de Barcelona, 08193 Bellaterra, Spain, Departament de Química Física and Centre Especial de Recerca en Química Teòrica, Universitat de Barcelona, Diagonal 647, 08028 Barcelona, Spain, and Departament de Química Inorgànica and Centre Especial de Recerca en Química Teòrica, Universitat de Barcelona, Diagonal 647, 08028 Barcelona, Spain

Received March 6, 2000

With the goal of understanding how the nature of the tridentate macrocyclic supporting ligand influences the relative stability of isomeric $\mu\text{-}\eta^2\text{:}\eta^2\text{-peroxo-}$ and $\text{bis}(\mu\text{-oxo})\text{dicopper}$ complexes, a comparative study was undertaken of the O_2 reactivity of Cu(I) compounds supported by the 10- and 12-membered macrocycles, 1,4,7- $\text{R}_3\text{-1,4,7-triazacyclododecane}$ (R_3TACD ; $\text{R} = \text{Me, Bn, iPr}$) and 1,5,9-triisopropyl-1,5,9-triazacyclododecane (iPr_3TACDD). While the 3-coordinate complex $[(\text{iPr}_3\text{TACDD})\text{Cu}]\text{SbF}_6$ was unreactive with O_2 , oxygenation of $[(\text{R}_3\text{TACD})\text{Cu}(\text{CH}_3\text{CN})]\text{X}$ ($\text{R} = \text{Me}$ or Bn ; $\text{X} = \text{ClO}_4^-$ or SbF_6^-) at -80°C yielded $\text{bis}(\mu\text{-oxo})$ species $[(\text{R}_3\text{TACD})_2\text{Cu}_2(\mu\text{-O})_2]\text{X}_2$ as revealed by UV–vis and resonance Raman spectroscopy. Interestingly, unlike the previously reported system supported by 1,4,7-triisopropyl-1,4,7-triazacyclononane (iPr_3TACN), which yielded interconverting mixtures of peroxo and $\text{bis}(\mu\text{-oxo})$ compounds (Cahoy, J.; Holland, P. L.; Tolman, W. B. *Inorg. Chem.* **1999**, *38*, 2161), low-temperature oxygenation of $[(\text{iPr}_3\text{TACD})\text{Cu}(\text{CH}_3\text{CN})]\text{SbF}_6$ in a variety of solvents cleanly yielded a $\mu\text{-}\eta^2\text{:}\eta^2\text{-peroxo}$ product, with no trace of the $\text{bis}(\mu\text{-oxo})$ isomer. The peroxo complex was characterized by UV–vis and resonance Raman spectroscopy, as well as an X-ray crystal structure (albeit of marginal quality due to disorder problems). Intramolecular attack at the $\alpha\text{-C-H}$ bonds of the substituents was indicated as the primary decomposition pathway of the oxygenated compounds through examination of the decay kinetics and the reaction products, which included $\text{bis}(\mu\text{-hydroxo})\text{-}$ and $\mu\text{-carbonato-dicopper}$ complexes that were characterized by X-ray diffraction. A rationale for the varying results of the oxygenation reactions was provided by analysis of (a) the X-ray crystal structures and electrochemical behavior of the Cu(I) precursors and (b) the results of theoretical calculations of the complete oxygenated complexes, including all ligand atoms, using combined quantum chemical/molecular mechanics (integrated molecular orbital molecular mechanics, IMOMM) methods. The size of the ligand substituents was shown to be a key factor in controlling the relative stabilities of the peroxo and $\text{bis}(\mu\text{-oxo})$ forms, and the nature of this influence was shown by both theory and experiment to depend on the ligand macrocycle ring size.

Introduction

The development of a detailed mechanistic understanding of dioxygen activation by metalloproteins continues to be an important objective in bioinorganic chemistry research, both because of the general significance of oxidase and oxygenase structure/function relationships in biology and because knowledge of O_2 binding and activation pathways may inform efforts to invent new synthetic oxidation catalysts.¹ Through in-depth

study of the reactions of O_2 with Cu(I) complexes, for example, important insights into how the O_2 molecule may coordinate to and subsequently be activated by copper sites in biology have been obtained.² In particular, a pathway by which the dioxygen O–O bond may be broken and formed within a dimetal protein active site was identified in studies of the oxygenation of $[(\text{iPr}_3\text{TACN})\text{Cu}(\text{CH}_3\text{CN})]^+$ ($\text{iPr}_3\text{TACN} = 1,4,7\text{-triisopropyl-1,4,7-triazacyclononane}$).^{2b,3} Under certain conditions, the reaction yields rapidly equilibrating mixtures of isomeric $\mu\text{-}\eta^2\text{:}\eta^2\text{-peroxo-}$ and $\text{bis}(\mu\text{-oxo})\text{dicopper}$ cores in ratios that depend on solvent, temperature, and counterions (Scheme 1).⁴

* E-mail: salvarez@kripto.qui.ub.es, tolman@chem.umn.edu.

[†] University of Minnesota.

[‡] Universitat Autònoma de Barcelona.

[§] Departament de Química Física and Centre Especial de Recerca en Química Teòrica, Universitat de Barcelona.

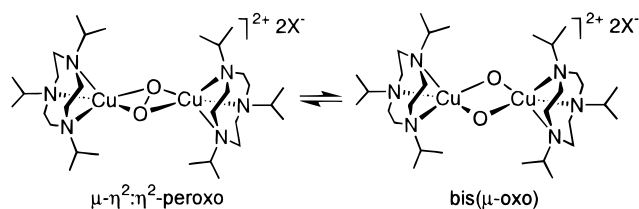
^{||} Departament de Química Inorgànica and Centre Especial de Recerca en Química Teòrica, Universitat de Barcelona.

(1) Selected reviews: (a) Solomon, E. I.; Sundaram, U. M.; Machonkin, T. E. *Chem. Rev.* **1996**, *96*, 2563–2605. (b) Klinman, J. P. *Chem. Rev.* **1996**, *96*, 2541. (c) Que, L., Jr. *Chem. Rev.* **1996**, *96*, 2607–2624. (d) Wallar, B. J.; Lipscomb, J. D. *Chem. Rev.* **1996**, *96*, 2625. (e) Sono, M.; Roach, M. P.; Dawson, J. H. *Chem. Rev.* **1996**, *96*, 2841. (f) Ferguson-Miller, S.; Babcock, G. T. *Chem. Rev.* **1996**, *96*, 2889. (g) *Cytochrome P450: Structure, Mechanism, and Biochemistry*, 2nd ed.; Ortiz de Montellano, P. R., Ed.; Plenum Press: New York, 1995.

(2) Recent reviews: (a) Karlin, K. D.; Zuberbühler, A. D. In *Bioinorganic Catalysis*, 2nd ed.; Reedijk, J., Ed.; Marcel Dekker: Inc.: New York, 1999; pp 469–534. (b) Tolman, W. B. *Acc. Chem. Res.* **1997**, *30*, 227. (c) Blackman, A. G.; Tolman, W. B. In *Metal-Oxo and Metal-Peroxo Species in Catalytic Oxidations*; Meunier, B., Ed.; Structure & Bonding Vol. 97; Springer-Verlag: Berlin, 2000; pp 179–211. (d) Kopf, M.-A.; Karlin, K. D. In *Biomimetic Oxidations Catalyzed by Transition Metal Complexes*; Meunier, B., Ed.; Imperial College Press: London, 2000; pp 309–362.

(3) Halfen, J. A.; Mahapatra, S.; Wilkinson, E. C.; Kaderli, S.; Young, V. G., Jr.; Que, L., Jr.; Zuberbühler, A. D.; Tolman, W. B. *Science* **1996**, *271*, 1397.

Scheme 1

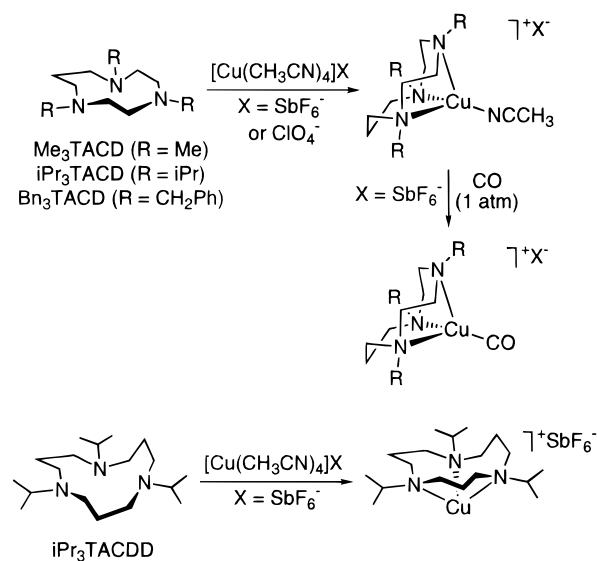


Studies of this system, as well as other related ones,⁵ have raised important questions about the potential involvement of the peroxo/bis(μ -oxo) interconversion in biological and catalytic oxidations and about the relative reactivity of each isomer toward hydrocarbon substrates. A significant underlying issue concerns how the supporting ligand influences the relative stability of the isomeric cores. From previous work it is clear that the nature of the substituents on the capping TACN unit influences the oxygenation chemistry significantly. Thus, with benzyl- or methyl-substituted TACN ligands^{5e,f,6} or with a ligand containing two $i\text{Pr}_2\text{TACN}$ units closely tethered by a $-\text{CH}_2-\text{CH}_2-$ chain,⁷ only bis(μ -oxo) complex formation is observed. More complicated mixtures of intramolecular peroxo and intermolecular (dimer-of-dimer or oligomeric) bis(μ -oxo) compounds result with xyllyl tethers.⁸ A survey of these results led to the hypothesis that the basis for the observed behavior for the TACN-supported systems is steric in nature.^{2b} According to this notion, large groups on TACN inhibit formation of the more compact bis(μ -oxo) core characterized by $\text{Cu}\cdots\text{Cu}$ distances of ~ 2.8 Å and favor $\mu\text{-}\eta^2\text{:}\eta^2$ -peroxo compound formation ($\text{Cu}\cdots\text{Cu} = \sim 3.5$ Å); with smaller N-substituents, collapse to the bis(μ -oxo) core is facilitated. In ligands comprising linked TACN units, tether length appears to be the controlling factor. Theoretical studies of the model system $[(\text{NH}_3)_3\text{Cu}(\text{O}_2)\text{Cu}(\text{NH}_3)_3]^{2+}$ and related species^{5f,9} have provided many electronic structural insights and, in particular, have indicated that the

disposition of the N-donor groups also must be considered in any effort to understand the relative stability of the isomers. Experimental verification of the role of N-donor disposition in ligand systems that vary only in this regard is lacking, however, and previous theoretical studies have not adequately considered the aforementioned key role of the N-donor substituents.

We report herein a combined experimental/theoretical examination of the $\text{Cu}(\text{I})/\text{O}_2$ reactivity of compounds supported by ligands comprising 10- and 12-membered macrocycles, $\text{R}_3\text{-TACD}$ (TACD = 1,4,7-triazacyclododecane) and $i\text{Pr}_3\text{TACDD}$ (TACDD = 1,5,9-triazacyclododecane) (Scheme 2).¹⁰ Through

Scheme 2



this work, and with reference to previous studies of the TACN system,^{3,4,5e,f,6} variation of both N-donor disposition and substituent size in a closely related series was accomplished, thus enabling a detailed analysis of their conjoined roles in determining the relative stabilities of the peroxo and bis(μ -oxo) isomers. We have found that disparities in supporting ligand macrocycle ring and substituent size correlate with acute differences in the nature of the products obtained in the oxygenations. To rationalize these findings, we have analyzed X-ray crystallographic data for the $\text{Cu}(\text{I})$ precursors and results of theoretical calculations of the complete oxygenated complexes, including all ligand atoms, using combined quantum chemical/molecular mechanics (integrated molecular orbital molecular mechanics, IMOMM) methods.

Results and Discussion

Copper(I) Complexes. (a) Synthesis. The complexes $[(\text{R}_3\text{-TACD})\text{Cu}(\text{CH}_3\text{CN})]\text{X}$ ($\text{R} = \text{Me}$, $i\text{Pr}$, or Bn ; $\text{X} = \text{ClO}_4^-$ or SbF_6^-) and $[(i\text{Pr}_3\text{TACDD})\text{Cu}]\text{SbF}_6$ (Scheme 2) were synthesized by mixing the appropriate salt of $[\text{Cu}(\text{CH}_3\text{CN})_4]^+$ with R_3TACD or $i\text{Pr}_3\text{TACDD}$, ligands which were prepared in turn from their respective parent macrocycles¹⁰ by known procedures¹¹ or by precedented alkylation methods.¹² The indicated formulations for the complexes are supported by the combined NMR and FTIR spectroscopic, mass spectrometric, elemental analysis, and (except for the Bn_3TACD case) X-ray crystallographic data (vide

- (4) (a) Cahoy, J.; Holland, P. L.; Tolman, W. B. *Inorg. Chem.* **1999**, *38*, 2161. (b) Holland, P. L.; Tolman, W. B. *Coord. Chem. Rev.* **1999**, *190–192*, 855.
- (5) (a) Mahadevan, V.; Hou, Z.; Cole, A. P.; Root, D. E.; Lal, T. K.; Solomon, E. I.; Stack, T. D. P. *J. Am. Chem. Soc.* **1997**, *119*, 11996. (b) Obias, H. V.; Lin, Y.; Murthy, N. N.; Pidcock, E.; Solomon, E. I.; Ralle, M.; Blackburn, N. J.; Neuhold, Y. M.; Zuberbühler, A. D.; Karlin, K. D. *J. Am. Chem. Soc.* **1998**, *120*, 12960. (c) Itoh, S.; Nakao, H.; Berreau, L. M.; Kondo, T.; Komatsu, M.; Fukuzumi, S. *J. Am. Chem. Soc.* **1998**, *120*, 2890. (d) Pidcock, E.; DeBeer, S.; Obias, H. V.; Hedman, B.; Hodgson, K. O.; Karlin, K. D.; Solomon, E. I. *J. Am. Chem. Soc.* **1999**, *121*, 1870. (e) Mahadevan, V.; DuBois, J. L.; Hedman, B.; Hodgson, K. O.; Stack, T. D. P. *J. Am. Chem. Soc.* **1999**, *121*, 5583. (f) Henson, M. J.; Mukherjee, P.; Root, D. E.; Stack, T. D. P.; Solomon, E. I. *J. Am. Chem. Soc.* **1999**, *121*, 10332. (g) Hayashi, H.; Fujinami, S.; Nagatomo, S.; Ogo, S.; Suzuki, M.; Uehara, A.; Watanabe, Y.; Kitagawa, T. *J. Am. Chem. Soc.* **2000**, *122*, 2124. (h) Decker, H.; Dillinger, R.; Tuczec, F. *Angew. Chem., Int. Ed.* **2000**, *39*, 1591.
- (6) Mahapatra, S.; Halfen, J. A.; Wilkinson, E. C.; Pan, G.; Wang, X.; Young, V. G., Jr.; Cramer, C. J.; Que, L., Jr.; Tolman, W. B. *J. Am. Chem. Soc.* **1996**, *118*, 11555.
- (7) Mahapatra, S.; Young, V. G., Jr.; Tolman, W. B. *Angew. Chem., Int. Ed.* **1997**, *36*, 130.
- (8) Mahapatra, S.; Kaderli, S.; Llobet, A.; Neuhold, Y.-M.; Palanché, T.; Halfen, J. A.; Young, V. G., Jr.; Kaden, T. A.; Que, L., Jr.; Zuberbühler, A. D.; Tolman, W. B. *Inorg. Chem.* **1997**, *36*, 6343.
- (9) (a) Cramer, C. J.; Smith, B. A.; Tolman, W. B. *J. Am. Chem. Soc.* **1996**, *118*, 11283. (b) Bérces, A. *Inorg. Chem.* **1997**, *36*, 4831. (c) Eisenstein, O.; Getlicherman, H.; Giessner-Prettre, C.; Maddaluno, J. *Inorg. Chem.* **1997**, *36*, 3455. (d) Liu, X.-Y.; Palacios, A. A.; Novoa, J. J.; Alvarez, S. *Inorg. Chem.* **1998**, *37*, 1202. (e) Bernardi, F.; Bottoni, A.; Casadio, R.; Fariselli, P.; Rigo, A. *Int. J. Quantum Chem.* **1996**, *58*, 109. (f) Bernardi, F.; Bottoni, A.; Casadio, R.; Fariselli, P.; Rigo, A. *Inorg. Chem.* **1996**, *35*, 5207. (g) Flock, M.; Pierloot, K. *J. Phys. Chem. A* **1999**, *103*, 95. (h) Lind, T.; Siegbahn, P. E. M.; Crabtree, R. H. *J. Phys. Chem. B* **1999**, *103*, 1193.

- (10) (a) Koyama, H.; Yoshino, T. *Bull. Chem. Soc. Jpn.* **1972**, *45*, 481. (b) Richman, J. E.; Atkins, T. J. *J. Am. Chem. Soc.* **1974**, *96*, 2268.
- (11) Geraldes, C. F. G. C.; Sherry, A. D.; Marques, M. P. M.; Alpoim, M. C.; Cortes, S. *J. Chem. Soc., Perkin Trans.* **1991**, 137.
- (12) Haselhorst, G.; Stoetzel, S.; Strassburger, A.; Walz, W.; Wieghardt, K.; Nuber, B. *J. Chem. Soc., Dalton Trans.* **1993**, 83.

Table 1. Electrochemical Data for Cu(I) Complexes^a and $\nu(\text{CO})$ Bands in FTIR Spectra of Derived Carbonyl Complexes

complex	$E_{1/2}$ (V) ^b	ΔE_p (V)	$\nu(\text{CO})$ (cm ⁻¹) ^c
[(iPr ₃ TACN)Cu(CH ₃ CN)] ⁺	0.57	0.51	2067 ^d
[(iPr ₃ TACD)Cu(CH ₃ CN)] ⁺	0.60	0.18	2063
[(Me ₃ TACD)Cu(CH ₃ CN)] ⁺	0.40	0.39	2086
[(Bn ₃ TACD)Cu(CH ₃ CN)] ⁺	0.44	0.50	2074
[(iPr ₃ TACDD)Cu] ⁺	(0.91) ^e		

^a Conditions: 9:1 (v/v) CH₂Cl₂/CH₃CN, 0.1 M (Bu₄N)(PF₆), scan rate 0.100 V/s, Pt electrode. ^b Reported versus SCE. ^c Carbonyl stretching frequencies of CO adducts of indicated complexes, measured as KBr pellets. ^d Reference 15. ^e E_{pa} value (irreversible oxidation).

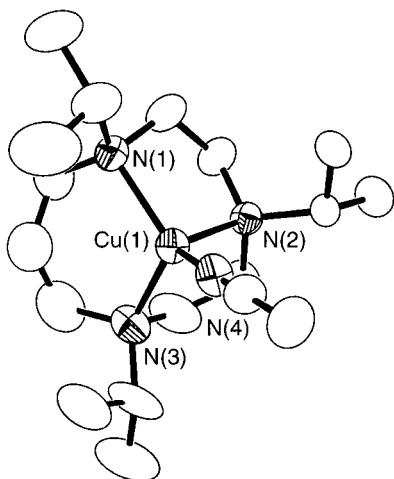


Figure 1. Representation of the cationic portion of the X-ray structure of [(iPr₃TACD)Cu(CH₃CN)]SbF₆, shown as 50% ellipsoids with H atoms omitted for clarity. Selected bond distances (Å) and angles (deg): Cu(1)–N(1) 2.102(6), Cu(1)–N(2) 2.137(5), Cu(1)–N(3) 2.144(7), Cu(1)–N(4) 1.895(6), N(4)–Cu(1)–N(1) 130.4(3), N(4)–Cu(1)–N(2) 117.5(2), N(1)–Cu(1)–N(2) 87.3(2), N(4)–Cu(1)–N(3) 120.3(3), N(1)–Cu(1)–N(3) 101.6(3), N(2)–Cu(1)–N(3) 87.7(2).

infra). Metal complexation of the respective ligands was particularly apparent in ¹H NMR spectra, where broad, often overlapping peaks for the macrocycle backbone hydrogens in the free macrocycle were replaced by a greater number of downfield-shifted and sharpened peaks resulting from conformational “locking” upon Cu(I) binding. In one case, [(iPr₃TACD)Cu(CH₃CN)]SbF₆, an analysis of 2D ¹H NMR data allowed detailed assignment of the ¹H NMR spectrum to be made (cf. COSY spectrum in Figure S1).¹³ The carbon monoxide adducts [(R₃TACD)Cu(CO)]SbF₆ (R = Me, iPr, or Bn) were prepared in straightforward fashion (Scheme 2). Corresponding $\nu(\text{CO})$ values (Table 1) are compared to electrochemical data below in an attempt to assess the relative electron-donating/withdrawing capabilities of the substituents.

(b) X-ray Crystal Structures. The cationic portions of the structures of [(iPr₃TACD)Cu(CH₃CN)]SbF₆, [(Me₃TACD)Cu(CH₃CN)]ClO₄, and [(iPr₃TACDD)Cu]ClO₄ are shown in Figures 1, 2, and 3, respectively. For comparison, the structure of [(iPr₃TACN)Cu(CH₃CN)]BPh₄ was also solved (Figure 4). Selected crystallographic data are listed in Table 2; see Supporting Information for complete listings. Consideration of the structural parameters of these compounds reveals features of potential importance for understanding their disparate reactivities with O₂.

While all of the compounds exhibit tridentate, facial coordination of their respective macrocyclic ligands, the structure

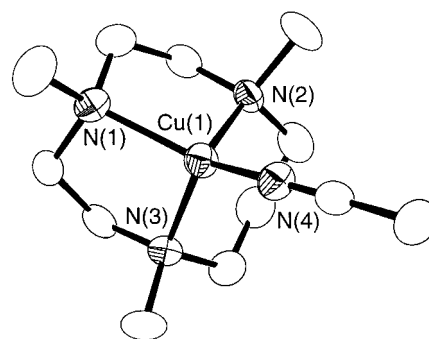


Figure 2. Representation of the cationic portion of the X-ray structure of [(Me₃TACD)Cu(CH₃CN)]ClO₄, shown as 50% ellipsoids with H atoms omitted for clarity. Selected bond distances (Å) and angles (deg): Cu(1)–N(1) 2.088(5), Cu(1)–N(2) 2.124(6), Cu(1)–N(3) 2.136(6), Cu(1)–N(4) 1.862(5), N(4)–Cu(1)–N(1) 141.2(2), N(4)–Cu(1)–N(2) 115.7(2), N(1)–Cu(1)–N(2) 86.3(2), N(4)–Cu(1)–N(3) 121.7(2), N(1)–Cu(1)–N(3) 86.4(2), N(2)–Cu(1)–N(3) 92.5(2).

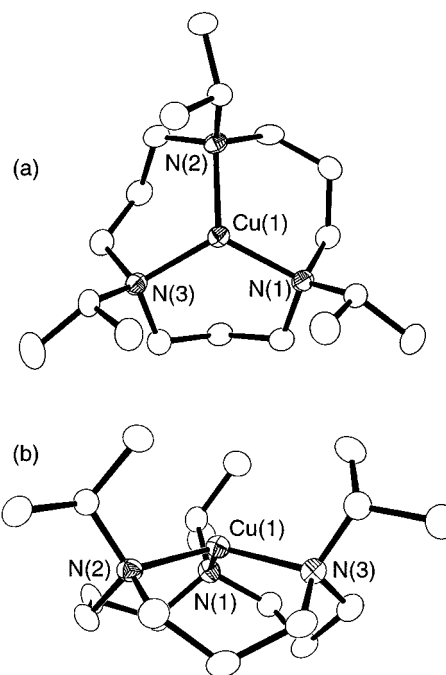


Figure 3. Two representations of the cationic portion of the X-ray structure of [(iPr₃TACDD)Cu]ClO₄, shown as 50% ellipsoids with H atoms omitted for clarity. Selected bond distances (Å) and angles (deg): Cu(1)–N(1) 2.019(2), Cu(1)–N(2) 2.022(2), Cu(1)–N(3) 2.026(2), N(1)–Cu(1)–N(2) 114.53(9), N(1)–Cu(1)–N(3) 116.96(9), N(2)–Cu(1)–N(3) 113.09(8).

of [(iPr₃TACDD)Cu]ClO₄ is unique because of the absence of a CH₃CN coligand. The Cu(I) ion adopts a 3-coordinate geometry with Cu–N bond distances slightly shorter [2.019(2)–2.026(2) Å range] than observed in the other 4-coordinate compounds. Residing deep within the 12-membered macrocycle but 0.46 Å above the N1–N2–N3 plane, the metal geometry is best described as pyramidal; the N–Cu–N angles are similar (113–117° range) and sum to 345° (vs 360° expected for a trigonal planar site). The coordination geometry in this compound would be expected to greatly favor the Cu(I) over the Cu(II) state, which was verified experimentally by a lack of reactivity with O₂ and a high reduction potential (vide infra).

Roughly similar 4-coordinate, C_{3v}-distorted tetrahedral geometries are adopted by the four remaining complexes of the R₃TACD and iPr₃TACN ligands. The Cu–N_{amine} bond distances fall within a narrow range typical for these types of compounds

Table 2. X-ray Crystallographic Data

	[(iPr ₃ TACD)-Cu(CH ₃ CN)]SbF ₆	[(Me ₃ TACD)-Cu(CH ₃ CN)]ClO ₄	[(iPr ₃ TACDD)-Cu]ClO ₄	[(iPr ₃ TACN)-Cu(CH ₃ CN)]BPh ₄	[(Me ₃ TACD) ₂ -Cu ₂ (OH) ₂](ClO ₄) ₂	[(iPr ₃ TACD) ₂ -Cu ₂ (CO ₃)](BPh ₄) ₂ ·4CH ₂ Cl ₂ ·1.5C ₃ H ₆ O
empirical formula	C ₁₈ H ₃₈ CuF ₆ N ₄ Sb	C ₁₂ H ₂₆ ClCuN ₄ O ₄	C ₁₈ H ₃₉ ClCuN ₃ O ₄	C ₄₁ H ₅₆ BCuN ₄	C ₂₀ H ₄₈ Cl ₂ Cu ₂ N ₆ O ₁₀	C _{89.5} H ₁₂₇ B ₃ Cl ₈ -Cu ₂ N ₆ O _{4.5}
fw	609.81	389.36	460.51	679.25	730.62	1791.27
cryst syst	orthorhombic	monoclinic	orthorhombic	monoclinic	monoclinic	triclinic
space group	<i>P2</i> ₁ <i>2</i> ₁ <i>2</i> ₁	<i>P2</i> ₁	<i>Pca2</i> ₁	<i>P2</i> ₁ / <i>n</i>	<i>P2</i> ₁ / <i>n</i>	<i>P1</i>
<i>a</i> (Å)	9.9638(4)	7.5134(1)	17.4559(3)	12.9986(3)	8.7398(6)	12.5429(2)
<i>b</i> (Å)	13.3049(6)	14.2737(3)	8.3552(1)	19.9770(3)	8.5565(6)	12.9911(2)
<i>c</i> (Å)	19.5424(9)	8.2653(2)	15.0250(3)	14.7452(1)	20.566(2)	28.0132(1)
α (deg)	90	90	90	90	90	85.0661(4)
β (deg)	90	98.264(1)	90	97.592(1)	95.705(1)	89.7265(8)
γ (deg)	90	90	90	90	90	88.4361(6)
<i>Z</i>	4	2	4	4	2	2
density (calcd; g cm ⁻³)	1.563	1.474	1.396	1.189	1.586	1.309
temp (K)	293(2)	173(2)	173(3)	173(2)	173(2)	173(2)
cryst size (mm)	0.35 × 0.25 × 0.22	0.26 × 0.21 × 0.06	0.40 × 0.19 × 0.06	0.35 × 0.15 × 0.15	0.40 × 0.30 × 0.08	0.38 × 0.29 × 0.05
abs coeff (mm ⁻¹)	1.917	1.418	1.146	0.608	1.623	0.755
θ range (deg)	1.85–25.03	2.49–25.11	2.33–25.01	1.73–25.04	1.99–25.03	0.73–25.01
reflns collected	13008	4498	10981	17612	7219	25779
indep reflns	4549	2845	3416	6575	2676	15039
params/restraints	271/24	204/1	250/1	484/0	181/0	1043/0
R1 [<i>I</i> > 2σ(<i>I</i>)] ^a	0.0461	0.0562	0.0285	0.0629	0.0561	0.0989
wR2 [<i>I</i> > 2σ(<i>I</i>)] ^b	0.1094	0.1561	0.0560	0.0968	0.1231	0.2259
GOF	1.040	1.075	1.074	1.094	1.097	1.055
largest diff features (e Å ⁻³)	0.437/−0.377	1.193/−0.444	0.213/−0.238	0.512/−0.322	0.756/−0.447	2.212/−0.982

^a R1 = Σ||*F*_o − |*F*_c||/Σ|*F*_o|. ^b wR2 = [Σ[w(*F*_o² − *F*_c²)/Σ[w(*F*_o²)]]^{1/2} where *w* = *q*/σ²(*F*_o²) + (*aP*)² + *bP*.

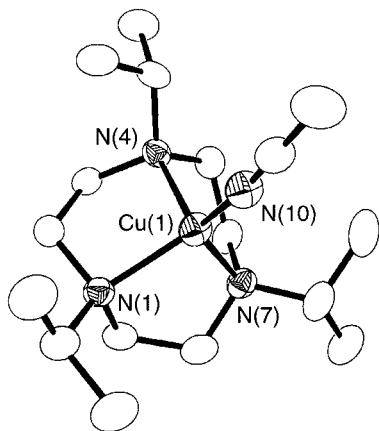


Figure 4. Representation of the cationic portion of the X-ray structure of [(iPr₃TACN)Cu(CH₃CN)]BPh₄, shown as 50% ellipsoids with H atoms omitted for clarity. Selected bond distances (Å) and angles (deg): Cu(1)–N(1) 2.113(3), Cu(1)–N(4) 2.151(3), Cu(1)–N(7) 2.147(3), Cu(1)–N(10) 1.865(3), N(10)–Cu(1)–N(1) 135.6(1), N(10)–Cu(1)–N(7) 129.4(1), N(1)–Cu(1)–N(7) 85.9(1), N(10)–Cu(1)–N(4) 118.3(1), N(1)–Cu(1)–N(4) 86.2(1), N(7)–Cu(1)–N(4) 85.4(1).

(2.09–2.15 Å)^{14,15} and the Cu–N_{nitrile} distances are short, as expected (range 1.86–1.90 Å). Despite these general similarities, specific comparisons between the pairs of complexes ligated by iPr₃TACD vs Me₃TACD (different substituents, same ring size) and iPr₃TACD vs iPr₃TACN (same substituents, different ring size) reveal important structural disparities.

First, the larger substituents in iPr₃TACD vs Me₃TACD result in greater encapsulation of and, thus, more hindered access to the Cu(I) ion (see space-filling drawings in Figure S2). Differences in the observed macrocycle ring conformations also

may be traced to substituent size variation. Following previously published analyses of TACD compounds (Figure S3),¹⁶ we assign the conformations of the two 5-membered and one 6-membered chelate rings within each of the R₃TACD complexes as δ,λ-chair (R = Me) and λ,λ-sofa (R = iPr). The former conformation matches that found previously to be most stable (lowest strain energy) for Co and Cu complexes of the parent TACD ligand.^{16a,b} Thus, whereas methyl substitution appears to have negligible effects on the conformational energetics of the coordinated TACD macrocycle, the finding of a different conformation in the iPr₃TACD case implicates more substantial conformational energy effects of the larger isopropyl substituents. Still, the energy differences between conformations are not large, since we observed a chair conformation for the 6-membered ring in a different complex of iPr₃TACD in the solid state (vide infra).

Second, while Cu–N distances are similar in the iPr₃TACN and iPr₃TACD complexes comprising identical substituents, the additional methylene unit in the macrocycle of the latter influences the disposition of the iPr groups. Thus, in [(iPr₃TACD)Cu(CH₃CN)]⁺, there is greater crowding about the CH₃CN ligand compared to the iPr₃TACN analogue. This difference between the two structures may be traced to differences in the position of the Cu ion relative to the planes defined by the macrocycle N-donor atoms and the iPr methine carbon atoms, respectively (Figure 5). The Cu ion in the iPr₃TACD case lies close to the N-donor plane (deeper inside this larger macrocycle) and approximately within the plane of the methine C atoms, whereas in the iPr₃TACN complex it is farther from the N-donor atom plane and 0.7 Å above the methine C atom plane. As a result, access of exogenous molecules or molecular fragments to the Cu ion in the iPr₃TACD case is more hindered than in the iPr₃TACN instance. This key difference provides a possible rationale for O₂ reactivity results described below.

(14) Chaudhuri, P.; Oder, K. *J. Organomet. Chem.* **1989**, 367, 249.
 (15) Halfen, J. A.; Mahapatra, S.; Wilkinson, E. C.; Gengenbach, A. J.; Young, V. G., Jr.; Que, L., Jr.; Tolman, W. B. *J. Am. Chem. Soc.* **1996**, 118, 763.

(16) (a) Dwyer, M.; Searle, G. H. *Aust. J. Chem.* **1981**, 34, 2025. (b) Chen, X.-M.; Yao, Y.-X.; Shi, K.-L.; Mak, T. C. W. *Aust. J. Chem.* **1995**, 48, 139. (c) DaCruz, M. F.; Zimmer, M. *Inorg. Chem.* **1998**, 37, 366.

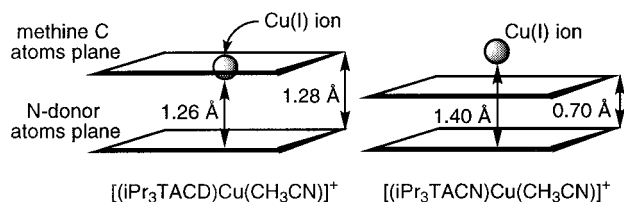


Figure 5. Comparison of the position of the Cu(I) ions in the X-ray structures of the indicated complexes relative to the planes defined by the macrocycle N-donor atoms and the *iPr* group methine carbon atoms.

(c) Electrochemistry. The results of cyclic voltammetry experiments are listed in Table 1, with representative CVs for the *iPr*₃TACDD, *iPr*₃TACD, and Me₃TACD cases provided in Figure S4. After numerous trials, the best results under a single set of conditions were obtained by using 9:1 (v/v) CH₂Cl₂/CH₃CN mixtures with 0.1 M (Bu₄N)(PF₆) as the supporting electrolyte. Nevertheless, large ΔE_p and unequal i_{pc} and i_{pa} values were observed in most instances, indicative of quasireversible behavior at best. Irreversible oxidation of [(*iPr*₃TACDD)Cu]⁺ was observed at high potential, consistent with stabilization of the Cu(I) state suggested by its trigonal structure and with major rearrangement upon oxidation. Comparison of the data acquired for the R₃TACD and *iPr*₃TACN systems is not particularly informative, although there appears to be a trend related to the size of the substituents; higher $E_{1/2}$ values were found for the *iPr*-substituted compounds than for the effectively smaller Me- and Bn-substituted cases. This trend does not correlate with the $\nu(\text{CO})$ values of the carbonyl complexes, which should be indicative of the amount of electron density at the metal center but do not track with the relative electron-donating properties of the ligand substituents. These seeming inconsistencies, in conjunction with the lack of cleanly reversible electrochemical behavior of the complexes in the CV experiments, has complicated efforts to relate their O₂ reactivity and redox properties.

Reactivity of Copper(I) Complexes with O₂. When solutions of [(R₃TACD)Cu(CH₃CN)]SbF₆ (R = Me or Bn) in CH₂Cl₂, THF, or acetone were oxygenated at –80 °C, an orange-brown color developed. The UV–vis and resonance Raman spectral features of the orange-brown solution were diagnostic for the formation of the bis(μ -oxo)dicopper core and clearly were inconsistent with the presence of its (μ - η^2 : η^2 -peroxo)dicopper isomer (Figures S5 and S6, and Table 3).^{3–8,17} Thus, we observed a pair of absorption features of similar high intensity ($\epsilon \sim 13000$ – $16000 \text{ M}^{-1} \text{ cm}^{-1}$) at ~ 310 and $\sim 415 \text{ nm}$ in UV–vis spectra and an ¹⁸O-sensitive feature at $\sim 600 \text{ cm}^{-1}$ ($\Delta^{18}\text{O} = 20$ – 25 cm^{-1}) in the resonance Raman spectrum ($\lambda_{\text{ex}} = 457 \text{ nm}$) that are signatures of the [Cu₂(μ -O)₂]²⁺ core.

In contrast, low-temperature oxygenation of [(*iPr*₃TACD)Cu(CH₃CN)]SbF₆ in CH₂Cl₂, THF, or acetone yielded a (μ - η^2 : η^2 -peroxo)dicopper complex only. This assignment was supported by UV–vis and resonance Raman spectroscopic data that are similar to those in the literature (Table 3);^{3,18} thus, diagnostic peroxo \rightarrow Cu(II) CT bands were observed in the absorption spectrum, and a $\nu(\text{O}=\text{O})$ at 739 cm^{-1} with the appropriate ¹⁸O shift was identified in the Raman spectrum. The $\nu(\text{O}=\text{O})$ is higher in energy than for the analogue supported by *iPr*₃TACN (713 cm^{-1}),¹⁷ but is similar to that seen for other systems with heterocyclic donor groups (cf. second and third entries in Table 3). Interestingly, unlike the case for the system supported by

*iPr*₃TACN where a small amount of bis(μ -oxo)dicopper isomer is apparent (UV–vis, resonance Raman) and is in equilibrium with the peroxo form,^{3,4} no bis(μ -oxo)dicopper form was seen for the *iPr*₃TACD case in any solvent. The cleanliness of the reaction to form the peroxo unit is illustrated in Figure S7, where absorption spectra for the systems capped by *iPr*₃TACD and *iPr*₃TACN are overlaid.

In view of the apparent absence of a bis(μ -oxo)dicopper species that would complicate crystallographic analysis,^{2b,5d} we attempted to determine the X-ray structure of the (μ - η^2 : η^2 -peroxo)dicopper complex supported by *iPr*₃TACD. After many trials, suitable crystals were obtained by using ligand with perdeuterated *iPr* substituents, BPh₄[–] counterions, and an acetone/butanone (1:1 v/v) solvent mixture at –80 °C. Although the structure is plagued by problems associated with solvent disorder and pseudosymmetry issues (see Supporting Information for details), the data were sufficient to confirm the presence of a planar (μ - η^2 : η^2 -peroxo)dicopper core capped by *iPr*₃TACD macrocycles (Figure 6). Detailed interpretation of bond distances is not warranted, but some important structural aspects are nonetheless worth noting. The data indicate an approximately planar (μ - η^2 : η^2 -peroxo)dicopper topology [Cu \cdots Cu 3.5 Å, O(1)–O(2), 1.4 Å] like those in the only other structurally characterized examples, [(Tp^{*iPr*}2Cu)₂(O₂)] [Cu \cdots Cu 3.560(3) Å, O(1)–O(2), 1.412(12) Å],^{18a} [LCu₂(O₂)](PF₆)₂ [Cu \cdots Cu 3.477(7) Å, O(1)–O(2), 1.485(8) Å],^{18d} and oxyhemocyanin [Cu \cdots Cu 3.6(2) Å, O(1)–O(2), 1.4(2) Å].¹⁹ However, whereas the Tp^{*iPr*}2 complex and oxyhemocyanin contain square pyramidal (SP) Cu(II) sites [$\tau = 0.03$ and 0.10 (av), respectively]²⁰ with the axial Cu–N bonds in an anti conformation (Figure 6c), each Cu(II) ion in the *iPr*₃TACD compound (Figure 6b) adopts a geometry significantly distorted (pseudorotated) from SP [$\tau = 0.30$ (av)]. Related distortions away from idealized SP Cu geometries were reported for [LCu₂(O₂)](PF₆)₂, although they probably are caused by constraints imposed by a tether between the capping N-donor units in this case.^{18d} Another aspect of the structure of the *iPr*₃TACD complex concerns the angle τ' between the pseudoaxial Cu–N bonds for each metal center, where $\tau' = 180^\circ$ and 0° for the extreme anti and syn conformations, respectively. The observed angle is 64° , an important distortion from the idealized conformations that are more closely approximated in known structures of other μ - η^2 : η^2 -peroxo- and bis(μ -oxo)dicopper compounds.^{5a,6,7}

Decomposition Reactions of Peroxo- and Bis(μ -oxo)-dicopper Complexes. The oxygenation products supported by the R₃TACD ligands decompose upon standing at temperatures above –80 °C. Detailed analyses of these reactions were not

- (18) Data for representative examples are discussed in the following: (a) Kitajima, N.; Fujisawa, K.; Fujimoto, C.; Moro-oka, Y.; Hashimoto, S.; Kitagawa, T.; Toriumi, K.; Tatsumi, K.; Nakamura, A. *J. Am. Chem. Soc.* **1992**, *114*, 1277. (b) Baldwin, M. J.; Root, D. E.; Pate, J. E.; Fujisawa, K.; Kitajima, N.; Solomon, E. I. *J. Am. Chem. Soc.* **1992**, *114*, 10421. (c) Mahapatra, S.; Halfen, J. A.; Wilkinson, E. C.; Que, L., Jr.; Tolman, W. B. *J. Am. Chem. Soc.* **1994**, *116*, 9785. (d) Kodera, M.; Katayama, K.; Tachi, Y.; Kano, K.; Hirota, S.; Fujinami, S.; Suzuki, M. *J. Am. Chem. Soc.* **1999**, *121*, 11006. L = 1,2-bis[2-(bis-(6-methyl-2-pyridyl)methyl)-6-pyridyl]ethane. (e) Solomon, E. I.; Tuzcek, F.; Root, D. E.; Brown, C. A. *Chem. Rev.* **1994**, *94*, 827. (f) Hu, Z.; Williams, R. D.; Tran, D.; Spiro, T. G.; Gorun, S. M. *J. Am. Chem. Soc.* **2000**, *122*, 3556.
- (19) (a) Magnus, K. A.; Hazes, B.; Ton-That, H.; Bonaventura, C.; Bonaventura, J.; Hol, W. G. *J. Proteins* **1994**, *19*, 302–309. (b) Magnus, K. A.; Ton-That, H.; Carpenter, J. E. *Chem. Rev.* **1994**, *94*, 727.
- (20) The parameter τ is defined in the following: Addison, A. W.; Rao, T. N.; Reedijk, J.; van Rijn, J.; Verschoor, G. C. *J. Chem. Soc., Dalton Trans.* **1984**, 1349. For an idealized square pyramidal geometry $\tau = 0$, while for an idealized trigonal bipyramidal arrangement $\tau = 1.0$.

(17) Holland, P. L.; Cramer, C. J.; Wilkinson, E. C.; Mahapatra, S.; Rodgers, K. R.; Itoh, S.; Taki, M.; Fukuzumi, S.; Que, L., Jr.; Tolman, W. B. *J. Am. Chem. Soc.* **2000**, *122*, 792.

Table 3. Spectroscopic Data for Products of Oxygenations of Selected Cu(I) Complexes

oxygenated complex	λ_{\max} (nm)	ϵ ($M^{-1} \text{ cm}^{-1}$)	Raman (cm^{-1}) ^a	$\Delta^{18}\text{O}$ (cm^{-1}) ^b	ref
$\{[(i\text{Pr}_3\text{TACN})\text{Cu}]_2(\mu\text{-}\eta^2\text{-}\eta^2\text{-O}_2)\}^{2+}$	366	22 500	713 ^c	41	17, 18c
	510	1 300			
$[(\text{LCu})_2(\mu\text{-}\eta^2\text{-}\eta^2\text{-O}_2)]^{2+ d}$	360	24 700	760	41	18d
	532	1 530			
$[(\text{Tp}^{\text{iPr}_2}\text{Cu})_2(\mu\text{-}\eta^2\text{-}\eta^2\text{-O}_2)]$	349	21 000	741	43	18a,b
	551	790			
$\{[(i\text{Pr}_3\text{TACD})\text{Cu}]_2(\mu\text{-}\eta^2\text{-}\eta^2\text{-O}_2)\}^{2+}$	380	22 000	739	43	this work
	520	2 300			
$\{[(i\text{Pr}_3\text{TACN})\text{Cu}]_2(\mu\text{-O})_2\}^{2+}$	324	11 000	589	22	3, 6
	418	13 000			
$\{[(\text{Bn}_3\text{TACN})\text{Cu}]_2(\mu\text{-O})_2\}^{2+}$	318	12 000	603/595 ^e	23	3, 6, 17
	430	14 000			
$\{[(\text{Me}_3\text{TACD})\text{Cu}]_2(\mu\text{-O})_2\}^{2+}$	304	16 000	595	20	this work
	404	16 200			
$\{[(\text{Bn}_3\text{TACD})\text{Cu}]_2(\mu\text{-O})_2\}^{2+}$	312	13 500	600	25	this work
	428	13 600			

^a O–O or Cu₂O₂ vibration in resonance Raman spectrum acquired on frozen solutions at 77 K with $\lambda_{\text{ex}} = 457$ or 514 nm. ^b Raman shift for complex prepared with ¹⁶O₂ minus Raman shift for complex prepared with ¹⁸O₂. ^c This value is corrected for a referencing error made in the original report; see ref 17 for details. ^d L = 1,2-bis[2-(bis(6-methyl-2-pyridyl)methyl)-6-pyridyl]ethane. ^e Fermi doublet in spectrum of ¹⁶O₂-derived sample.

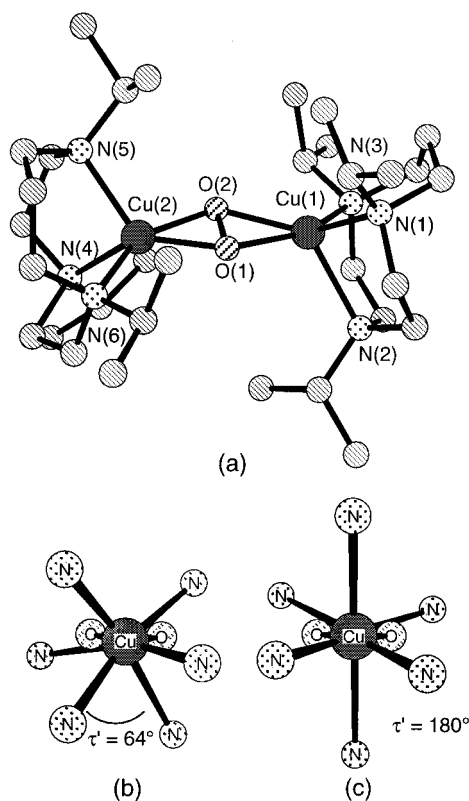


Figure 6. (a) Representation of the cationic portion of the X-ray structure of $[(d_{21}\text{-}i\text{Pr}_3\text{TACD})_2\text{Cu}_2(\mu\text{-}\eta^2\text{-}\eta^2\text{-O}_2)](\text{BPh}_4)_2 \cdot x\text{solvent}$. (b) View of the coordination spheres of the Cu(II) ions along the Cu...Cu vector, with τ' shown as the N–Cu–Cu–N torsional angle involving the pseudoaxial N donor atoms most distant from their respective Cu(II) ions. (c) View of the coordination spheres of the Cu(II) ions in $[\text{Tp}^{\text{iPr}_2}_2\text{Cu}_2(\mu\text{-}\eta^2\text{-}\eta^2\text{-O}_2)]$ along the Cu...Cu vector, with the indicated τ' value.^{16a}

undertaken, but selected data were acquired in order to draw comparisons to more thoroughly studied cases with other ligand systems reported previously.^{5,7,8,21} The decays of $\{[(\text{Me}_3\text{TACD})\text{Cu}]_2(\mu\text{-O})_2\}(\text{ClO}_4)_2$ and $\{[(i\text{Pr}_3\text{TACD})\text{Cu}]_2(\mu\text{-}\eta^2\text{-}\eta^2\text{-O}_2)\}(\text{ClO}_4)_2$ follow first-order kinetics with the activation parameters listed in Table 4 (determined via UV–vis monitoring; see Figure S8

Table 4. Activation Parameters for the Decomposition Reactions of Selected $\mu\text{-}\eta^2\text{-}\eta^2$ -Peroxo- and Bis($\mu\text{-oxo}$)dicopper Complexes^a

complex	ΔH^\ddagger (kcal mol ⁻¹)	ΔS^\ddagger (eu)	ref
$\{[(i\text{Pr}_3\text{TACN})\text{Cu}]_2(\mu\text{-}\eta^2\text{-}\eta^2\text{-O}_2)\}^{2+}$	13.5(5)	–12(1)	18c
$\{[(i\text{Pr}_3\text{TACD})\text{Cu}]_2(\mu\text{-}\eta^2\text{-}\eta^2\text{-O}_2)\}^{2+}$	11.9(5)	–20(1)	this work
$\{[(i\text{Pr}_3\text{TACN})\text{Cu}]_2(\mu\text{-O})_2\}^{2+}$	13.2(5)	–14(2)	21
$\{[(\text{Bn}_3\text{TACN})\text{Cu}]_2(\mu\text{-O})_2\}^{2+}$	13.0(5)	–13(2)	21
$\{[(\text{Me}_3\text{TACD})\text{Cu}]_2(\mu\text{-O})_2\}^{2+}$	12.2(5)	–24(2)	this work
$\{[\text{L}_{\text{Me}}\text{Cu}]_2(\mu\text{-O})_2\}^{2+ b}$	11.8(3)	–25(1)	5a

^a Determined from Eyring plots of first-order rate constants (Figure S8). ^b L_{Me} = N,N'-diethyl-N,N'-dimethyl-*trans*-(1R,2R)-diaminocyclohexane.

for Eyring plots). The observed behavior is quite similar to that noted previously for various TACN derivatives, suggesting similar pathways involving intramolecular attack of the peroxo or bis($\mu\text{-oxo}$) core at ligand substituent C–H bonds α to the N-donor atoms.

Although no effort was made to identify and quantify all of the decomposition products, small amounts of crystalline complexes were isolated and subjected to X-ray diffraction analysis. From the decay of the bis($\mu\text{-oxo}$) compound supported by Me₃TACD we isolated $\{[(\text{Me}_3\text{TACD})\text{Cu}]_2(\mu\text{-OH})_2\}(\text{ClO}_4)_2$ (Figure 7), which features a bis(hydroxo)dicopper(II) core typical for such species [Cu...Cu = 3.015 Å, Cu–OH = 1.93–1.95 Å]. The Cu(II) ions adopt slightly distorted SP geometries ($\tau = 0.17$), and the Me₃TACD macrocycles exhibit a similar conformation as in the Cu(I) complex (e.g., chair conformation for the 6-membered chelate ring). Another Cu(II) complex was isolated as a side product during attempts to crystallize the $\mu\text{-}\eta^2\text{-}\eta^2$ -peroxo complex supported by iPr₃TACD; its X-ray structure revealed it to be a μ -carbonato species apparently derived from fixation of atmospheric CO₂ by a bis(hydroxo) precursor (Figure 8). Numerous other dicopper carbonate complexes have been reported.²² The Cu(II) ions in this particular compound adopt trigonal bipyramidal geometries ($\tau = 0.82, 0.75$) with one of the amine donors and one of the carbonate oxygen atoms serving

(22) Some selected recent reports: (a) Escuer, A.; Mautner, F. A.; Peñalba, E.; Vicente, R. *Inorg. Chem.* **1998**, *37*, 4190. (b) Fusch, G.; Fusch, E. C.; Erxleben, A.; Hutterman, J.; Scholl, H.-J.; Lippert, B. *Inorg. Chim. Acta* **1996**, *252*, 167. (c) Sorrell, T. N.; Allen, W. E.; White, P. S. *Inorg. Chem.* **1995**, *34*, 952. (d) Kruger, P. E.; Fallon, G. D.; Moubaraki, B.; Berry, K. J.; Murray, K. S. *Inorg. Chem.* **1995**, *34*, 4808.

(21) Mahapatra, S.; Halfen, J. A.; Tolman, W. B. *J. Am. Chem. Soc.* **1996**, *118*, 11575.

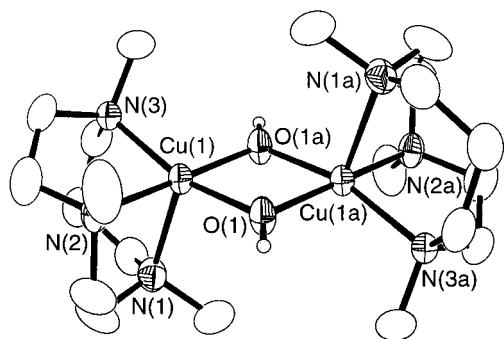


Figure 7. Representation of the cationic portion of the X-ray structure of $[(\text{Me}_3\text{TACD})_2\text{Cu}_2(\mu\text{-OH})_2](\text{ClO}_4)_2$, shown as 50% ellipsoids with all H atoms (except those placed on the bridging hydroxides) omitted for clarity. Selected bond distances (Å) and angles (deg): Cu(1)–O(1) 1.950(3), Cu(1)–O(1a) 1.933(3), Cu(1)–N(2) 2.041(4), Cu(1)–N(3) 2.060(4), Cu(1)–N(1) 2.272(4), Cu \cdots Cu 3.016(1), O(1a)–Cu(1)–O(1) 78.1(2), O(1a)–Cu(1)–N(2) 173.1(2), O(1)–Cu(1)–N(2) 97.0(2), O(1a)–Cu(1)–N(3) 96.8(2), O(1)–Cu(1)–N(3) 162.9(2), N(2)–Cu(1)–N(3) 86.6(2), O(1a)–Cu(1)–N(1) 102.7(2), O(1)–Cu(1)–N(1) 100.4(2), N(2)–Cu(1)–N(1) 82.9(2), N(3)–Cu(1)–N(1) 96.7(2), Cu(1)–O(1)–Cu(1a) 101.9(2).

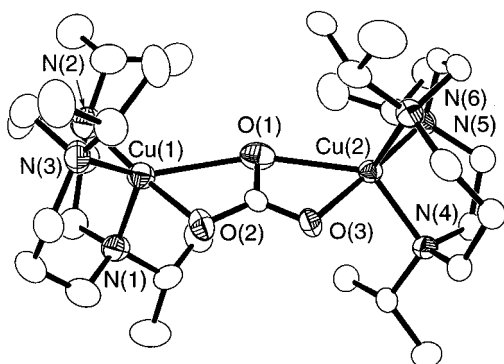


Figure 8. Representation of the cationic portion of the X-ray structure of $[(\text{iPr}_3\text{TACD})_2\text{Cu}_2(\mu\text{-CO}_3)](\text{X})_2 \cdot x \text{ solvate}$, shown as 50% ellipsoids with all H atoms omitted for clarity. Selected bond distances (Å): Cu(1)–O(2) 1.939(5), Cu(1)–N(2) 2.030(6), Cu(1)–N(3) 2.038(6), Cu(1)–N(1) 2.053(6), Cu(2)–O(3) 1.940(5), Cu(2)–N(5) 2.018(5), Cu(2)–N(4) 2.041(5), Cu(2)–N(6) 2.088(6), Cu(2)–O(1) 2.415(6). For bond angles, see Supporting Information.

as axial ligands in an arrangement different from an iPr_3TACN -supported analogue²³ that has SP Cu(II) geometries and a coordinated H_2O molecule. Unlike the Cu(I) complex of iPr_3TACD , the 6-membered chelate ring is in a chair conformation in the carbonate compound, indicating relatively similar energies for the sofa and chair conformers of this ligand when coordinated.

Theoretical Calculations. We evaluated via theoretical methods the relative energies and stereochemical differences between $\mu\text{-}\eta^2\text{:}\eta^2\text{-peroxo-}$ and $\text{bis}(\mu\text{-oxo})$ dicopper complexes supported by variously N-substituted tridentate 9- and 10-membered macrocycles. The primary objective was to determine how the size of the macrocycle and its N-donor substituents influence the structures and relative amounts of the peroxo and $\text{bis}(\mu\text{-oxo})$ products of the respective oxygenation reactions and, thus, rationalize the experimental findings discussed above. In the following discussion, we first consider unconstrained systems supported by NH_3 donors that serve as benchmarks for inherent electronic structure effects and then compare them to compounds containing the parent, unsubstituted TACN and TACD ligands. In so doing, we address the results of constraining the donor

Table 5. Relative Energies (kcal/mol) of the Peroxo and $\text{Bis}(\mu\text{-oxo})$ Isomers of $[\text{LCuO}_2\text{CuL}]^{2+}$ and of the Transition State for Their Interconversion, Calculated for Different Sets of Terminal Donors and at Different Computational Levels

entry	N-donors	transition			method	ref
		peroxo	state	$\text{bis}(\mu\text{-oxo})$		
1	$(\text{NH}_3)_3$	0	17.0	12.6	B3LYP	9d
2	$(\text{NH}_3)_3$	0		11.7	BP	9b
3	$(\text{NH}_3)_3$	0	18.7	14.4	B3LYP	9g
4	$(\text{NH}_3)_3$	0	24.2	19.9	bs-B3LYP	9g
5	$(\text{NH}_3)_3$	12.7		0	CASPT2	9g
6	$(\text{NH}_3)_3$	0		0.3	CASPT2/RHF	9a
7	TACN	0	17.0	11.3	B3LYP	c
8	TACN	0	7.9	0.2	BP	9b
9	TACD	0	15.8	7.2	B3LYP	c
10	Tp^a	0	8.8	2.9	BP	9b
11	Me_3TACD	0		21.5	B3LYP:MM3	c
12	iPr_3TACN	0		30.0 ^b	B3LYP:MM3	c
13	iPr_3TACD	0		34.5 ^b	B3LYP:MM3	c

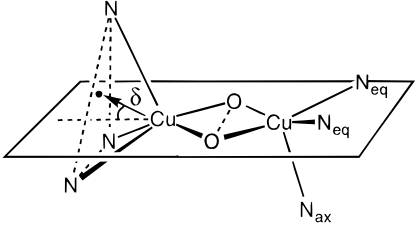
^a Tp = tris(pyrazolyl)hydroborate. ^b Not a minimum, evaluated at $\text{O}=\text{O} = 2.36$ Å. ^c This work.

atoms within these differently sized macrocycles. Then we will assess the steric effects associated with the presence of Me or iPr substituents at the donor atoms, as present in the *real* compounds, using combined molecular orbital/molecular mechanics IMOMM calculations.

The relative energies of the peroxo and $\text{bis}(\mu\text{-oxo})$ isomers at their optimized structures in the model compound $[(\text{NH}_3)_3\text{-CuO}_2\text{Cu}(\text{NH}_3)_3]^{2+}$ calculated at different levels of theory are given in Table 5 (entries 1–6). These previously published results indicate that the peroxo isomer generally is predicted to be more stable with DFT calculations, but when electron correlation is treated at the more precise CASPT2 level the relative stabilities are inverted.^{9b,d} The B3LYP calculations probably overestimate the relative stability of the $\mu\text{-peroxo}$ form. The use of broken-symmetry (bs) B3LYP calculations would be indicated for the formally Cu(II)₂ peroxo isomer, but these are expected to further stabilize it relative to the oxo-bridged form as indeed found by Flock and Pierloot (Table 5, entry 4).^{9g} We conclude from the combined available results that a quantitative interpretation of the calculated value for the difference in energy between the two isomers bound to NH_3 ligands is not warranted with the computational methodology available for the real molecules under study. The best we can say is that the two isomers probably differ in energy by less than 15 kcal/mol. Consequently, our emphasis will be on evaluating the qualitative effects of ligand structure on the relative stabilities of the two isomeric forms.

(a) Influences of Macrocyclic Ring Size. In a previous theoretical study important changes in the orientation of the terminal ligands were found to accompany the peroxo to $\text{bis}(\mu\text{-oxo})$ transformation.^{9d} In addition, the constraints imposed on the relative position of the donor atoms in a tridentate ligand were shown to affect the relative energies of the two isomers significantly. The main structural differences are summarized in Table 6, where δ reflects the orientation of the CuN_3 pyramids relative to the Cu_2O_2 plane as shown and Σ is the sum of the N–Cu–N bond angles that indicates the degree of pyramidalization around the Cu atoms. A simple way to summarize the calculated structural discrepancies is to consider two extreme situations for the coordination sphere of the copper atoms. At one extreme, a Cu(I) ion can be viewed as adopting a tetrahedral geometry with a $\eta^2\text{-O}_2$ ligand and the three N-donors occupying the four vertices (expected values for this arrangement are $\delta \approx 0^\circ$ and $\Sigma \approx 330^\circ$). At the other extreme, a Cu(III) ion adopts a square pyram-

(23) Schneider, J. L.; Young, V. G., Jr.; Tolman, W. B. *Inorg. Chem.* **1996**, *35*, 5410.

Table 6. Calculated Structural Parameters for the Peroxo and Oxo Isomers of $[\text{LCuO}_2\text{CuL}]^{2+}$ ($\text{L} = (\text{NH}_3)_3, \text{TACN}, \text{TACD}$)^a


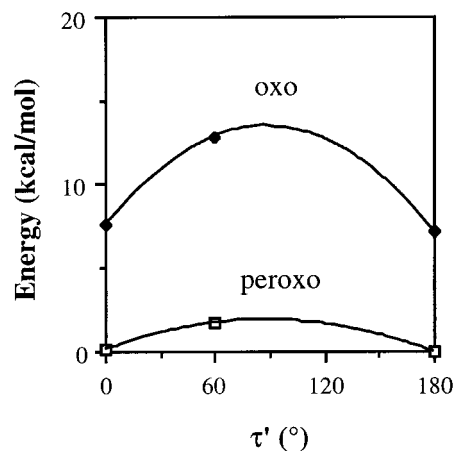
param	peroxo			bis(μ -oxo)		
	(NH ₃) ₃	TACD	TACN	(NH ₃) ₃	TACD	TACN
O—O	1.515	1.427	1.425	2.288	2.368	2.346
Cu—O	1.985	1.980	1.970	1.835	1.830	1.820
Cu—N _{eq}	2.055	2.044	2.064	2.003	2.004	2.008
Cu—N _{ax}	2.220	2.274	2.226	2.381	2.400	2.322
δ^b	19	21 (17)	14	29	23 (20)	19
Σ^c	313	273	256	289	263	251

^a All distances are given in angstroms; the angles δ and Σ are given in degrees. All values correspond to the anti conformation shown above ($\tau' = 180^\circ$), except for those in parentheses, which indicate the δ values for $\tau' \approx 0^\circ$ (all other values are practically the same for this case). ^b δ is defined by the drawing above. ^c Σ is the sum of the N—Cu—N bond angles.

idal geometry with one of the N donors occupying the axial position and two oxo anions in basal sites (expected parameters $\delta \geq 35^\circ$ and $\Sigma \approx 270^\circ$). The bis(μ -oxo) structure thus corresponds closely to the latter case, while the peroxo structure lies intermediate between the two extremes, consistent with its formal description and experimental data that indicate that it should be viewed as a (μ - η^2 : η^2 -peroxo)dicopper(II,II) unit.¹⁸

Comparison of the calculated structural data listed in Table 6 for the complexes $[\text{LCuO}_2\text{CuL}]^{2+}$, where $\text{L} = (\text{NH}_3)_3, \text{TACN}$, or TACD , indicates closely related geometric differences between the respective peroxo and bis(μ -oxo) forms. Thus, for each supporting ligand system, as the molecule converts from the peroxo to the bis(μ -oxo) structure (a) the Cu—O distances significantly shorten, (b) the Cu—N_{eq} distances decrease and the Cu—N_{ax} distances increase, resulting in much larger differences between the two types of Cu—N distances in the bis(μ -oxo) form, (c) the value of Σ decreases, and (d) the CuN₃ pyramids are bent further away from the Cu₂O₂ plane, as measured by an increase in δ . Importantly, the angle sum Σ for each isomeric form follows the series $\text{TACN} < \text{TACD} < \text{NH}_3$, consistent with the expected trend in ligand flexibilities; values of Σ and δ as well as their differences for the two isomers increase as the N-donor constraints decrease (NH₃ being the least and TACN being the most constrained).

In terms of energies, computational results for the compound $[(\text{TACN})\text{CuO}_2\text{Cu}(\text{TACN})]^{2+}$ (Table 5, entry 7) give nearly the same difference between the peroxo and the bis(μ -oxo) isomers as calculated previously at the same level of theory for the analogue supported by the monodentate NH₃ ligands (entry 1).^{9b} For the TACD complex (entry 9), however, the difference in energy between the two isomers is significantly smaller, a finding that we explain by the increased flexibility of the TACD macrocycle that can better adapt to the stereochemical changes required for the peroxo to bis(μ -oxo) transformation. This greater relative stabilization of the bis(μ -oxo) form for TACD compared to TACN contrasts with the experimental observation of only the peroxo isomer for $i\text{Pr}_3\text{TACD}$ and suggests that the nature of the N-donor substituents is an important determinant (vide infra). Finally, we note in passing that the calculated energies

**Figure 9.** Relative energy of $[(\text{TACD})\text{CuO}_2\text{Cu}(\text{TACD})]^{2+}$ as a function of the rotation angle τ' in the peroxo and bis(μ -oxo) forms. The rotation angle was kept fixed and the rest of the structure optimized for each point.

for the transition states indicate that the barriers for the cleavage of the O—O bond [peroxo \rightarrow bis(μ -oxo)] are quite similar with both macrocycles or the monodentate NH₃ ligands, but due to the divergent stabilities of the bis(μ -oxo) isomers the barriers for the reverse processes [bis(μ -oxo) \rightarrow peroxo] differ according to the series $\text{TACD} > (\text{NH}_3)_3 > \text{TACN}$.

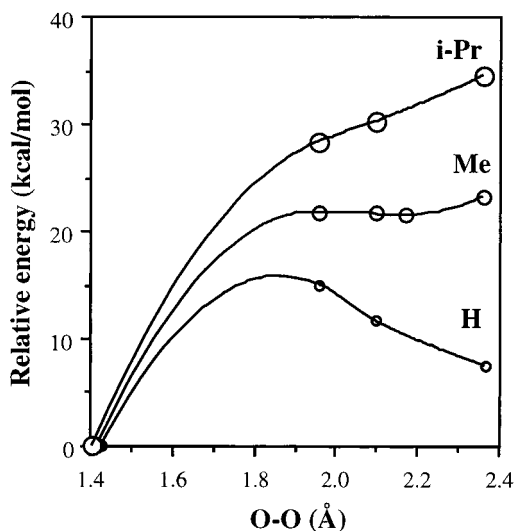
It is important to stress that the syn and anti conformations (i.e., N_{ax}—Cu—Cu—N_{ax} torsion angles $\tau' = 0$ and 180° , respectively) of both the peroxo and bis(μ -oxo) forms supported by TACD are essentially isoenergetic at the present level of calculation (energy difference less than 0.4 kcal/mol, Figure 9). Rotation between these two conformations affects the Cu—N distances; an excellent linear correlation (Figure S9) is found between the position of each Cu—N bond relative to the Cu₂O₂ plane (given by the N—Cu—Cu—O torsion angle) and the Cu—N distance, with the shortest distance (1.969 Å) corresponding to the Cu—N bond coplanar with the Cu₂O₂ ring and the longest one to the Cu—N bond perpendicular to the same plane (2.401 Å). Importantly, while the energy of the rotated conformation ($\tau' = 60^\circ$) for the peroxo isomer differs little from those of its syn and anti conformations, this rotated conformation for the bis(μ -oxo) form is about 5 kcal/mol less stable than its syn and anti ones. This point is relevant to the following discussion of substituent effects on the relative stabilities and structures of the TACN- and TACD-supported systems. Finally, we note that previous calculations on the model complex $[(\text{NH}_3)_6\text{Cu}_2(\mu\text{-O})_2]^{2+}$ with unconstrained monodentate ligands found syn and anti conformations of the oxo isomer to be almost isoenergetic at the DFT level, but a more accurate treatment of the electron correlation (CASPT2 level) predicted the syn conformation to be some 9 kcal/mol more stable.⁶

(b) Influences of N-Donor Substituents. The effects of the substituents in the TACD and TACN complexes were analyzed via combined molecular orbital/molecular mechanics IMOMM calculations (B3LYP:MM3), in which both of the entire macrocyclic ligands together with the Cu₂O₂ core were treated quantum-mechanically (QM) and the R groups at the six nitrogen donors were treated by molecular mechanics (MM) (see Experimental Section for details). In these calculations, the geometry of the full molecule is optimized by minimizing the total energy, which is the sum of the QM and MM contributions ($E_{\text{tot}} = E_{\text{QM}} + E_{\text{MM}}$). The MM term is mostly associated with the steric interactions between the substituents. In order to minimize such repulsions, the $[\text{LCuO}_2\text{CuL}]^{2+}$ core is somewhat

Table 7. Calculated Structural Parameters for the Peroxo and Bis(μ -oxo) Isomers of $[(R_3TACX)CuO_2Cu(R_3TACX)]^{2+}$, Where R = H, Me, or *iPr*^a

ligand/isomer	O···O	τ'	Cu–O	Cu–N _{eq}	Cu–N _{ax}	Σ	N···N ^c	C···C ^d	δ^e
TACD/peroxo	1.427	4	1.980	2.045	2.274	273	6.001		21 (17)
Me ₃ TACD/peroxo	1.416	11	1.990	2.065	2.272	275	5.952	3.985	18
<i>iPr</i> ₃ TACD/peroxo	1.403	44	2.012	2.067, 2.154	2.317, 2.394	276, 277	6.464	3.591	13
<i>iPr</i> ₃ TACD/peroxo (expt)	1.367	64	1.89	2.05	2.218	276, 281	5.930	3.620	12
TACD/bis(μ -oxo)	2.367	0	1.830	2.005	2.400	263	5.224		23 (20)
Me ₃ TACD/bis(μ -oxo)	2.169	31	1.832	2.068	2.366	264	5.506	3.768	16
<i>iPr</i> ₃ TACD/bis(μ -oxo)	2.360 ^b	58	1.84–1.89	2.064–2.265	2.372, 2.777	258, 264	5.695	3.497	16
TACN/peroxo	1.425	180	1.970	2.064	2.226	256			14
<i>iPr</i> ₃ TACN/peroxo	1.411	180	1.984	2.068, 2.115	2.247, 2.255	258, 260	6.465	4.295	12
TACN/bis(μ -oxo)	2.346	180	2.008	2.008	2.322	251	5.899	3.912	19
<i>iPr</i> ₃ TACN/bis(μ -oxo)	2.360 ^b	180	1.852, 1.844	2.086	2.452	249	5.803	3.904	16

^a All distances are given in angstroms; the angles δ and Σ are given in degrees. The angle δ is defined by the drawing above Table 6, Σ is the sum of the N–Cu–N bond angles, and τ' is the N_{ax}–Cu–Cu–N_{ax} torsion angle. ^b O···O distance frozen and the remaining parts of the structure optimized. ^c Shortest contact between the corresponding atoms of the two TACD ligands. ^d Shortest contact between the substituents of the two TACD ligands. ^e Values in parentheses correspond to the anti conformation ($\tau' = 180^\circ$).

**Figure 10.** Calculated (B3LYP/MM3) relative energy (ΔE_{tot}) for the R_3TACD complexes as a function of the O–O distance (all other parameters optimized for each distance).

distorted with respect to the analogous molecule with unsubstituted ligands, resulting in an increase in E_{QM} .

Only a minor distortion of the core in the peroxo form is induced by the presence of the Me groups on the TACD ligand, as reflected by a small increase of E_{QM} upon methyl substitution (1.3 kcal/mol). In contrast, the *iPr* groups impose severe distortions (see Table 7) and a large increase of E_{QM} (11.2 kcal/mol). The destabilization introduced by the substituents is more important as the O···O distance increases, the Cu···Cu distance simultaneously decreases, and the substituents of the two macrocycles approach each other as the peroxo core isomerizes to the bis(μ -oxo) form. This trend is illustrated in Figure 10, where the total IMOMM energies for the various TACD compounds are represented as a function of the O···O distance, taking as the zero for each compound the energy of its most stable peroxo form (except for the peroxo form, the O···O distance was frozen, and the rest of the molecular structure reoptimized). Note that the destabilization of the bis(μ -oxo) form relative to the peroxo increases with the size of the substituent, *iPr* > Me > H (Table 5, entries 9, 11, and 13). As a result, the formation of the peroxo isomer is most favored when the core is supported by the *iPr*₃TACD ligand, in good agreement with experiment. We note in passing that the TACD macrocycle presents the same conformation in all cases with no significant differences in its bonding parameters.

To gain some understanding of the reasons for the changes in relative stability upon substitution, we separately analyze the QM and MM contributions to the total energy. The energy partition for the complexes of Me₃TACD, *iPr*₃TACD, and *iPr*₃TACN is presented in Figure 11 as a function of the O···O distance (ΔE_{QM} = squares, ΔE_{MM} = triangles, total energy = circles), together with the calculated electronic energies for the corresponding unsubstituted macrocycles (crosses). As might be intuitively obvious, the steric energy reflecting the interligand repulsions within each complex becomes greater as the O···O distance increases and the Cu···Cu distance simultaneously decreases. Interestingly, however, the extent of MM destabilization in the process peroxo \rightarrow bis(μ -oxo) differs little between Me₃TACD, *iPr*₃TACD, and *iPr*₃TACN. Instead, a more important issue is the difference between the QM energies of the complexes with N-alkylated ligands and those analogues with the respective unsubstituted, parent macrocycle. In each case, the QM destabilization of the bis(μ -oxo) form increases upon N-substitution, with the greatest difference being that between the complexes supported by *iPr*₃TACD and TACD (Figure 11).

An analysis of the structural perturbations attending N-substitution in the series of TACD-supported systems helps us understand these QM energy effects (Table 7). We note initially the excellent agreement between the main structural features of the *iPr*₃TACD-capped peroxo isomer obtained from IMOMM calculations with the experimental data. Second, the calculations indicate that the incorporation of bulkier substituents produces an increasing destabilization of the syn conformation ($\tau' = 0^\circ$), resulting in rotated conformations with torsion angles in the range $11^\circ < \tau' < 56^\circ$. This effect is enhanced as the macrocyclic ligands approach each other (i.e., O···O distance increases) and as the N-substituent size increases (*iPr* > Me > H). The qualitative agreement in the large torsion angle for the calculated and experimentally determined peroxo structures supported by *iPr*₃TACD is a key finding. Evidently, a significant reorganization of the Cu coordination sphere reflected by an increase in τ' results from steric repulsions between substituents of the capping ligands. The reorganization is most drastic for the case of the bis(μ -oxo) form supported by *iPr*₃TACD and results in strong desymmetrization of the complex that becomes apparent when the two oxygen atoms are separated by 2.10 Å. One of the copper atoms presents a coordination sphere characteristic of bis(μ -oxo) isomers, with a relatively small Σ value (260°) and a large difference between the long and the two short Cu–N distances. The other copper atom, however, has the same value of Σ as in the peroxo isomer (276°) and a smaller difference

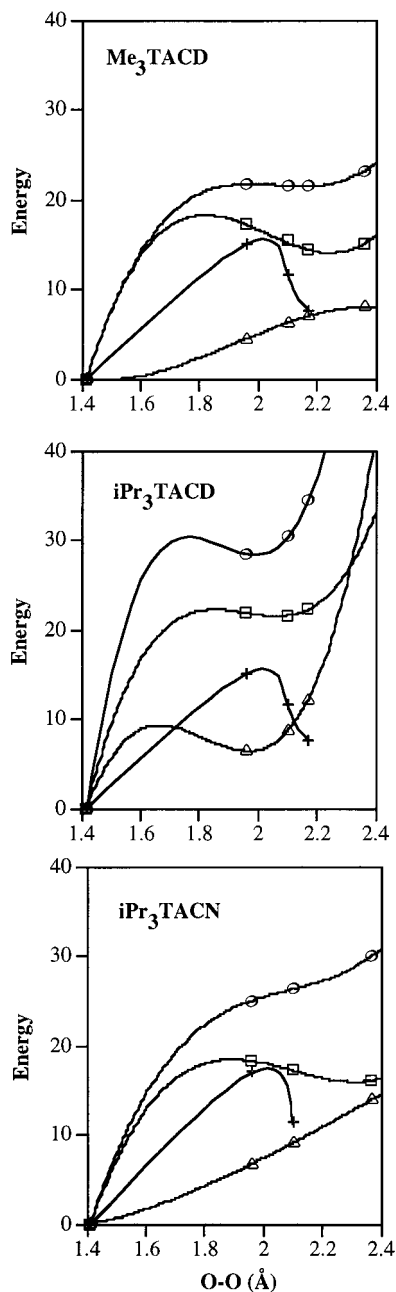


Figure 11. Calculated relative energy (IMOMM, kcal/mol) for the $[(R_3TACX)Cu(O_2)Cu(R_3TACX)]$ complexes as a function of the O—O distance (ΔE_{QM} = squares, ΔE_{MM} = triangles, ΔE_{tot} = circles), together with the calculated ΔE_{QM} values for the corresponding unsubstituted macrocycles (crosses). The energy at the shortest O—O distance is taken as the zero for each curve.

between the long and short Cu—N distances. We infer that these structural distortions (large τ' and disparate Σ values) underlie the large calculated QM destabilization of this bis(μ -oxo) isomer relative to those capped by less sterically encumbered R_3TACD ligands, thus explaining the experimental observation of only the peroxo form for the iPr_3TACD system.

Comparison of the results of IMOMM calculations for the systems supported by iPr_3TACN and iPr_3TACD enables evaluation of the experimental findings, namely, the formation of both peroxo and bis(μ -oxo) isomers for the former and only the peroxo form for the latter. These differences in Cu/O₂ reactivity are particularly interesting because the systems only differ by virtue of one methylene unit in their capping ligand backbone. As described above, consideration of the results of calcu-

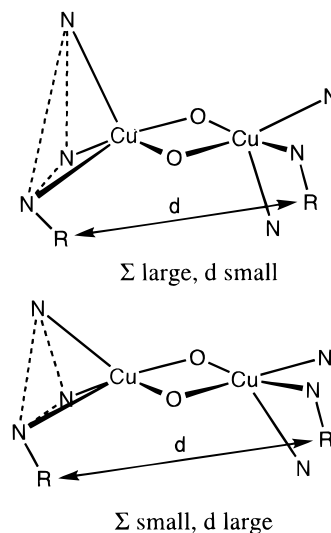


Figure 12. Illustration of the relationship between the sum of N—Cu—N angles (Σ) and the distance between the N-substituents in the bis(μ -oxo)dicopper complexes.

lations with the unsubstituted TACN and TACD ligands suggests that the greater flexibility of the larger macrocycle preferentially stabilizes its bis(μ -oxo) isomer. However, consideration of Figure 11 reveals that it is the lesser QM destabilization of the TACN derivative by the isopropyl group N-substitution that makes the bis(μ -oxo) form more stable with this macrocycle. Hence, the QM destabilization of the bis(μ -oxo) form that is introduced by the isopropyl groups in iPr_3TACN is calculated to be 5.9 kcal/mol, compared to 11.2 kcal/mol for the iPr_3TACD ligand. What is the structural basis for this difference? One divergence between the bis(μ -oxo) topologies for the two ligand systems is the torsional angle, which for iPr_3TACN is $\tau' = 180^\circ$ (an anti conformation) versus $\tau' = 56^\circ$ for its ring-expanded counterpart (Table 7). However, it would be expected that closer interligand substituent contacts between groups in the equatorial positions and correspondingly greater energetic destabilization would attend the 180° angle for the iPr_3TACN case, arguing against this feature being responsible for the observed energetic discrepancy. Instead, we see that the angle sum Σ is significantly smaller for TACN than for TACD at a similar O—O distance, regardless of the nature of the substituent. In other words, TACN is a tridentate ligand with a smaller cone angle, hence the nitrogen donor atoms of each macrocyclic ligand and their substituents are farther away from each other (Figure 12) as illustrated by longer N \cdots N and C \cdots C contacts at the same O—O distance (Table 7). The steric effects of the iPr groups are thus magnified in TACD relative to TACN, with the result being a greater destabilization of the more congested, smaller bis(μ -oxo) core for the ligand with the larger macrocyclic backbone. These effects are corroborated by the X-ray structural data obtained for the Cu(I) precursor complexes (vide supra).

Summary and Conclusions

Through a combination of experimental and theoretical studies, we have obtained new insights into the influences of ligand structure on the relative stability of the isomeric (μ - η^2 : η^2 -peroxo)- and bis(μ -oxo)dicopper cores. We synthesized and fully characterized a set of Cu(I) complexes of N-substituted macrocycles with 12- and 10-membered rings, iPr_3TACDD and R_3TACD ($R = Me, Bn, \text{ and } iPr$), respectively, and we compared their O₂ reactivity with that of previously reported systems

supported by the 9-membered-ring congeners, R₃TACN. The lack of O₂ reactivity for the iPr₃TACDD system may be rationalized by considering the structure of its Cu(I) complex, which due to its trigonal geometry has a prohibitive redox potential. For the systems capped by Me₃TACD and Bn₃TACD, clean formation of bis(μ -oxo) complexes was observed, whereas sole generation of a peroxo complex was seen when iPr₃TACD was used. This peroxo complex was characterized by X-ray crystallography, which revealed interesting distortions of the metal coordination spheres that include a relative orientation ($\tau' = 64^\circ$) of the pseudoaxial N-donors intermediate between syn ($\tau' = 0^\circ$) and anti ($\tau' = 180^\circ$). Sole production of the peroxo form upon oxygenation of the Cu(I) complex of iPr₃TACD contrasts with the behavior found previously for the iPr₃TACN-supported system, where mixtures of rapidly interconverting peroxo and bis(μ -oxo) isomers were found whose ratios depended on solvent and temperature.

In order to rationalize this important disparity in O₂ reactivity that resulted from a relatively small ligand structural difference (a single methylene unit in the macrocycle), we analyzed the X-ray structures of the Cu(I) precursors and performed comparative theoretical studies using combined quantum mechanics/molecular mechanics methods. Although the calculations did not necessarily yield good quantitative estimates of the relative energy of the oxo and peroxo isomers (vide supra), they provided an excellent indication of how that relative energy is influenced by ligand reorganization, by the macrocyclic nature of the ligand, and by the steric effects of the ligand substituents. The calculations showed that an important rearrangement of the N-donor orientation of the TACN and TACD ligands relative to the Cu₂O₂ core occurs as the peroxo converts to the bis(μ -oxo) form, as previously found with monodentate NH₃ model ligands.^{9d} While the increased flexibility of the TACD ligand results in a somewhat more stable bis(μ -oxo) isomer than for the TACN case, the destabilization of the bis(μ -oxo) relative to the peroxo isomer by iPr group N-substitution is greater for TACD than TACN due to cone angle differences. A large part of the destabilization of the bis(μ -oxo) form is not purely steric, but instead results from distortion of the central [N₃CuO₂-CuN₃]²⁺ core and rotation of the two Cu(macrocycle) units ($0^\circ < \tau' < 180^\circ$) that may be traced to avoidance of close interligand contacts between the iPr groups. The IMOMM computational results for [(iPr₃TACD)CuO₂Cu(iPr₃TACD)]²⁺ are in excellent agreement with the main structural features deduced from the X-ray diffraction data. In addition, the conclusions concerning the divergent steric effects of the iPr groups on the different macrocycles are corroborated by the X-ray structural data for the Cu(I) precursors, which show clear differences in steric accessibility due to shifted orientations of the N-donor substituents on the TACN and TACD macrocycles.

Finally, we recognize that the present computations predict the peroxo isomer to be more stable than the bis(μ -oxo) one in all cases, including those supported by Me₃TACX (X = D or N) that in reality yield bis(μ -oxo) compounds only. This consistent overestimation of the energy of the bis(μ -oxo) form may result from a lack of inclusion of solvent effects; we recall that for the model compound [(NH₃)₃CuO₂Cu(NH₃)₃]²⁺ Cramer et al. found^{6,9a} that application of a simple solvent dielectric stabilizes a bis(μ -oxo) isomer by 5.6–8.4 kcal/mol relative to the peroxo. Experimental studies of the iPr₃TACN system have illustrated the importance of solvent, temperature, and counterion effects and suggest that quantitative assessment via theory of the stabilities of the isomeric Cu₂O₂ cores will necessitate inclusion of entropic and/or “second-sphere” influences.⁴ Not-

withstanding this issue, the comparative calculations presented here do allow the relative influences of key aspects of ligand structure on the peroxo/bis(μ -oxo) ratio to be understood.

Experimental Section

General Procedures. All reagents and solvents were obtained from commercial sources and were used as received unless stated otherwise. Solvents were dried according to published procedures²⁴ and distilled under N₂ prior to use. Air-sensitive reactions were performed either in a Vacuum Atmospheres inert-atmosphere glovebox or by standard Schlenk and vacuum line techniques. The starting materials [Cu(CH₃CN)₄]X (X = ClO₄⁻, SbF₆⁻),²⁵ 1,4,7-triazacyclododecane (TACD),¹⁰ 1,5,9-triazacyclododecane (TACDD),¹⁰ 1,4,7-trimethyl-1,4,7-triazacyclododecane (Me₃TACD),¹¹ and 1,4,7-triisopropyl-1,4,7-triazacyclononane¹² were synthesized using published procedures. Elemental analyses were performed by Atlantic Microlabs of Norcross, GA. Resonance Raman spectra were collected on a Spex 1403 spectrometer interfaced with a DM3000 data collection system or on an Acton 506 spectrometer using a Princeton Instruments LN/CCD-1100-PB/UVAR detector and ST-1385 controller interfaced with Winspec software. A Spectra-Physics 2030-15 argon ion laser at a power of roughly 40 mW was employed to give the excitation wavelength at 514.5 or 457.9 nm. The spectra were obtained at 77 K using a 135° backscattering geometry; samples were frozen onto a gold-plated copper coldfinger in thermal contact with a dewar containing liquid nitrogen. Raman shifts were referenced to the intense solvent features at 702 (CH₂Cl₂) or 797 (acetone) cm⁻¹. Other instrumentation and conditions for physicochemical characterization of new compounds were used as described previously.¹⁵

1,4,7-Triisopropyl-1,4,7-triazacyclododecane (iPr₃TACD). The reagent 2-bromopropane (11.0 g, 0.0894 mol) was added to a solution of TACD (2.70 g, 0.0189 mol) in toluene (30 mL). The colorless reaction mixture was allowed to reflux for 2 h and over time became light yellow. Powdered KOH (~10 g) was added to the yellow solution, and the mixture was refluxed overnight. The solution was then cooled to room temperature and filtered, and the residue was washed with toluene (30 mL). The combined filtrates were dried, and the solvent was removed under reduced pressure, to yield a light yellow oil, which was distilled (~85 °C, 0.25 Torr), to give the product as a clear oil (2.11 g, 42%). ¹H NMR (CDCl₃, 300 MHz): δ 0.91 (d, *J* = 6.6 Hz, 18H), 1.38 (q, *J* = 5.7 Hz, 2H), 2.40–2.43 (m, 4H), 2.59–2.62 (m, 4H), 2.67 (t, *J* = 5.7 Hz, 4H), 2.82 (h, *J* = 6.6 Hz, 3H) ppm. ¹³C{¹H} NMR (CDCl₃, 75 MHz): δ 50.6, 50.4, 49.5, 49.3, 46.9, 27.9, 18.5, 17.9 ppm. Anal. Calcd for C₁₆H₃₅N₃: C, 71.31; H, 13.09; N, 15.60. Found: C, 71.26; H 12.97, N, 15.49. The deuterated ligand *d*₂₁-iPr₃-TACD was prepared analogously to iPr₃TACD using *d*₇-2-bromopropane. ¹H NMR (CDCl₃, 300 MHz): δ 1.40 (q, *J* = 5.7 Hz, 2H), 2.40–2.48 (m, 4H), 2.60–2.72 (m, 8H) ppm.

1,4,7-Tribenzyl-1,4,7-triazacyclododecane (Bn₃TACD). Benzyl chloride (1.32 g, 0.0104 mol) was added to a solution of TACD (0.372 g, 2.60 mmol) in toluene (15 mL). The light yellow solution was stirred for 2 h. Powdered KOH (~4 g) was added to the solution, and the mixture was refluxed overnight. The solution was then cooled to room temperature and filtered, and the residue was washed with toluene (20 mL). The combined filtrates were dried, and the solvent was removed under reduced pressure, to yield a light yellow oil (0.955 g, 88%). The ligand was used without further purification. ¹H NMR (CDCl₃, 300 MHz): δ 1.60–1.72 (m, 2H), 2.42–2.65 (m, 6H), 2.69–2.91 (m, 6H), 3.23 (s, 2H), 3.55 (s, 4H), 7.05–7.22 (m, 15H) ppm.

1,5,9-Triisopropyl-1,5,9-triazacyclododecane (iPr₃TACDD). This ligand was prepared analogously to iPr₃TACD but with TACDD as the starting material. The resulting light yellow oil was distilled (~120 °C, 0.25 Torr), to give the product as a colorless oil (55%). ¹H NMR (CDCl₃, 300 MHz): δ 0.91 (d, *J* = 6.6 Hz, 18H), 1.47 (q, *J* = 6.3 Hz, 6H), 2.40 (t, *J* = 6.3 Hz, 12H), 2.83 (h, *J* = 6.6 Hz, 3H) ppm. ¹³C{¹H} NMR (CDCl₃, 75 MHz): δ 48.5, 44.7, 21.9, 18.5 ppm. Anal. Calcd for C₁₈H₃₉N₃: C, 72.65; H, 13.22; N, 14.13. Found: C, 72.74; H, 13.32; N, 14.00.

(24) Perrin, D. D.; Armarego, W. L. F. *Purification of Laboratory Chemicals*; Pergamon Press: New York, 1988.

(25) Kubas, G. J. *Inorg. Synth.* **1979**, *19*, 90–92; **1990**, *28*, 68.

[(iPr₃TACD)Cu(CH₃CN)]SbF₆. In the glovebox, solid [Cu(CH₃CN)₄]SbF₆ (0.172 g, 0.371 mmol) was added to a stirred solution of iPr₃TACD (0.100 g, 0.372 mmol) in CH₃CN (2 mL). The solution was stirred for 30 min before being added to Et₂O (20 mL), which resulted in the deposition of the product as a white powder (0.181 g, 80%). ¹H NMR (CD₃CN, 500 MHz): δ 1.19 (d, *J* = 6.5 Hz, 6H), 1.20 (d, *J* = 6.5 Hz, 6H), 1.21 (d, *J* = 6.5 Hz, 6H), 1.58–1.70 (m, 1H), 1.88–2.00 (m, 4H), 2.50–2.64 (m, 6H), 2.76–2.98 (m, 6H), 3.0 (h, *J* = 6.5 Hz, 2H), 3.1 (h, *J* = 6.5 Hz, 1H) ppm. ¹³C{¹H} NMR (CD₂Cl₂, 75 MHz): δ 58.6, 55.2, 51.9, 50.1, 28.4, 18.9, 18.6, 18.3, 2.7 ppm (observed 9 out of 11 expected signals). FTIR (KBr, cm⁻¹): 2980, 2911, 2883, 2853, 2267 (C≡N), 1495, 1472, 1461, 1376, 1270, 1183, 1161, 1147, 1123, 1071, 1032, 955, 937, 738, 658 (SbF₆⁻). FAB-MS (MNBA): *m/e* (relative intensity) 373 ([M - SbF₆]⁺, 3), 332 ([M - CH₃CN - SbF₆]⁺, 100). Anal. Calcd for CuC₁₈H₃₈N₄SbF₆: C, 35.45; H, 6.28; N, 9.19. Found: C, 35.65; H, 6.48; N, 9.14. [(iPr₃TACD)Cu(CH₃CN)]ClO₄ was prepared analogously to [(iPr₃TACD)Cu(CH₃CN)]SbF₆, except by using [Cu(CH₃CN)₄]ClO₄ (81%). ¹H NMR (CD₃CN, 300 MHz): δ 1.18 (d, *J* = 6.6 Hz, 6H), 1.19 (d, *J* = 6.6 Hz, 6H), 1.22 (d, *J* = 6.6 Hz, 6H), 1.58–1.70 (m, 1H), 1.88–2.00 (m, 4H), 2.50–2.64 (m, 6H), 2.76–2.98 (m, 6H), 3.0 (h, *J* = 3.9 Hz, 2H), 3.1 (h, *J* = 3.9 Hz, 1H) ppm.

[(d₂₁-iPr₃TACD)Cu(CH₃CN)]BPh₄. In the glovebox, solid NaBPh₄ (0.158 g, 0.462 mmol) was added to a stirred solution of d₂₁-iPr₃TACD (0.149 g, 0.514 mmol) and CuCl (0.046 g, 0.465 mmol) in CH₃CN (2 mL). After the cloudy white solution had been stirred for 30 min, it was filtered through a Celite pad. Additional CH₃CN (5 mL) was used to wash the Celite pad, and the combined filtrates were brought to dryness under reduced pressure, yielding a white powder. Recrystallization with CH₃CN/Et₂O (1:20) gave white feathery crystals (0.317 g, 86%). ¹H NMR (CD₂Cl₂, 300 MHz): δ 1.62–1.72 (m, 1H), 1.83–1.97 (m, 4H), 2.47–2.58 (m, 6H), 2.73–2.94 (m, 6H), 6.91 (t, *J* = 7.2 Hz, 4H), 7.06 (t, *J* = 7.2 Hz, 8H), 7.32–7.38 (m, 8H) ppm. ¹³C{¹H} NMR (CD₂Cl₂, 75 MHz): δ 164.1, 135.9, 125.6, 121.7, 51.9, 50.1, 41.7, 29.9, 21.6, 17.9, 17.0, 2.3 ppm (observed 12 out of 15 expected signals). FTIR (KBr, cm⁻¹): 3054, 3037, 2983, 2927, 2853, 2259 (C≡N), 2244, 1582, 1480, 1457, 1429, 1295, 1213, 1185, 1147, 1051, 845, 742, 729 (BPh₄⁻), 702 (BPh₄⁻), 604. FAB-MS (MNBA) *m/e* (relative intensity) 394 ([M - BPh₄]⁺, 2), 248 ([M - CH₃CN - BPh₄]⁺, 100).

[(Me₃TACD)Cu(CH₃CN)]SbF₆. In the glovebox, solid [Cu(CH₃CN)₄]SbF₆ (0.060 g, 0.11 mmol) was added to a stirred solution of Me₃TACD (0.030 g, 0.16 mmol) in CH₃CN (2 mL). After the solution had been stirred for 10 min, it was added to Et₂O (20 mL), resulting in the precipitation of the product as a white powder (0.053 g, 78%). ¹H NMR (CD₂Cl₂, 500 MHz): δ 1.68–1.76 (m, 1H), 1.94–2.04 (m, 1H), 2.20 (s, 3H), 2.40–2.46 (m, 2H), 2.58 (s, 6H), 2.64–2.74 (m, 7H), 2.74–2.90 (m, 6H) ppm. ¹³C{¹H} NMR (CD₂Cl₂, 75 MHz): δ 59.0, 55.8, 55.3, 49.2, 48.9, 25.7, 2.6 ppm (observed 7 out of 8 expected signals). FTIR (KBr, cm⁻¹): 2971, 2866, 2813, 2362, 2342, 2266 (C≡N), 1494, 1468, 1367, 1273, 1042, 768, 662 (SbF₆⁻). FAB-MS (MNBA): *m/e* (relative intensity) 289 ([M - SbF₆]⁺, 10), 248 ([M - CH₃CN - SbF₆]⁺, 100). X-ray-quality crystals were obtained with the perchlorate salt, which was synthesized in a similar fashion.

[(Bn₃TACD)Cu(CH₃CN)]SbF₆. This was prepared analogously to [(iPr₃TACD)Cu(CH₃CN)]SbF₆, except by using Bn₃TACD (72%) in CH₂Cl₂. The light yellow solid was further purified by recrystallization from CH₂Cl₂/Et₂O (1:20). ¹H NMR (CD₂Cl₂, 300 MHz): δ 1.66–1.79 (m, 1H), 1.90–2.60 (m, 1H), 2.23 (s, 3H), 2.40–2.58 (m, 4H), 2.62–2.88 (m, 6H), 3.06–3.20 (m, 2H), 3.67 (s, 2H), 3.78 (s, 4H), 7.24–7.31 (m, 4H), 7.37–7.47 (m, 11H) ppm. ¹³C{¹H} NMR (CD₂Cl₂, 75 MHz): δ 135.5, 133.5, 131.4, 131.1, 128.6, 128.4, 128.3, 65.1, 63.8, 56.3, 54.6, 49.7, 24.7, 2.87 ppm (observed 14 out of 16 expected signals). Anal. Calcd for CuC₃₀H₃₈N₄SbF₆: C, 47.79; H, 5.08; N, 7.43. Found: C, 48.34; H, 5.18; N, 6.99.

[(iPr₃TACDD)Cu]SbF₆. This was prepared analogously to [(iPr₃TACD)Cu(CH₃CN)]SbF₆, except by using iPr₃TACDD in CH₂Cl₂ (74%). ¹H NMR (CD₂Cl₂, 300 MHz): δ 1.21 (d, *J* = 6.6 Hz, 18H), 1.76–1.98 (m, 6H), 2.74 (qd, *J* = 2.4, 7.2 Hz, 6H), 2.94 (qd, *J* = 2.4, 8.1 Hz, 6H), 3.20 (h, *J* = 6.6 Hz, 3H) ppm. ¹³C{¹H} NMR (CDCl₃, 75 MHz): δ 56.1, 56.0, 25.8, 18.6 ppm. Anal. Calcd for C₁₈H₃₉CuF₆N₃Sb: C, 36.22; H, 6.59; N, 7.04. Found: C, 36.47; H, 6.61; N, 7.09.

X-ray-quality crystals were obtained with the similarly prepared perchlorate salt by using CH₂Cl₂/Et₂O (vapor diffusion).

[(iPr₃TACD)Cu(CO)]SbF₆. Solid [(iPr₃TACD)Cu(CH₃CN)]SbF₆ (0.063 g, 0.103 mmol) was dissolved in acetone (5 mL) in a Schlenk flask. Carbon monoxide was bubbled through the light yellow solution for 5 min. After the solution was allowed to equilibrate for an additional 10 min, the solvent was removed under reduced pressure, yielding a white powder. The product was reprecipitated from acetone/Et₂O (1:20) to give a white powder (0.053 g, 85%). ¹H NMR (CD₂Cl₂, 300 MHz): δ 1.27 (d, *J* = 6.6 Hz, 6H), 1.30 (d, *J* = 6.6 Hz, 6H), 1.33 (d, *J* = 6.6 Hz, 6H), 1.73–1.86 (m, 1H), 1.98–2.14 (m, 1H), 2.64–2.82 (m, 6H), 2.92–3.08 (m, 6H), 3.17 (h, *J* = 6.6 Hz, 2H), 3.23 (h, *J* = 6.6 Hz, 2H) ppm. ¹³C{¹H} NMR (CD₂Cl₂, 75 MHz): δ 60.4, 56.8, 53.1, 52.9, 51.0, 27.2, 20.2, 19.3, 18.2 ppm (observed 9 out of 10 expected signals). FTIR (KBr, cm⁻¹): 2980, 2939, 2879, 2063 (C≡O), 1494, 1465, 1393, 1377, 1349, 1214, 1178, 1142, 1063, 1035, 915, 864, 746, 707, 657 (SbF₆). Anal. Calcd for CuN₃C₁₇H₃₅OSbF₆: C, 34.21; H, 5.88; N, 7.04. Found: C, 33.64; H, 5.77; N, 7.12.

[(Me₃TACD)Cu(CO)]SbF₆. This compound was prepared analogously to [(iPr₃TACD)Cu(CO)]SbF₆, except by using [(Me₃TACD)Cu(CH₃CN)]SbF₆ (84%). ¹H NMR (CD₂Cl₂, 500 MHz): δ 1.78–1.82 (m, 1H), 2.07–2.16 (m, 1H), 2.46–2.52 (m, 2H), 2.75 (s, 6H), 2.80–2.85 (m, 4H), 2.88 (s, 3H), 2.98–3.06 (m, 6H) ppm. ¹³C{¹H} NMR (CD₂Cl₂, 75 MHz): δ 58.9, 57.0, 55.1, 50.8, 50.7, 24.3 ppm (observed 6 out of 7 expected signals). FTIR (KBr, cm⁻¹): 2949, 2880, 2086 (C≡O), 1474, 1365, 1262, 1106, 1065, 1032, 762, 658 (SbF₆). Anal. Calcd for CuN₃C₁₁H₂₃OSbF₆: C, 25.77; H, 4.52; N, 8.20. Found: C, 25.96; H, 4.52; N, 8.13.

[(Bn₃TACD)Cu(CO)]SbF₆. This compound was prepared analogously to [(iPr₃TACD)Cu(CO)]SbF₆, except by using [(Bn₃TACD)Cu(CH₃CN)]SbF₆ (91%). ¹H NMR (CD₂Cl₂, 500 MHz): δ 1.74–1.88 (m, 1H), 1.96–2.18 (m, 1H), 2.62–2.76 (m, 4H), 2.76–2.96 (m, 4H), 2.08–3.32 (m, 4H), 3.83 (s, 2H), 2.86 (s, 4H), 7.12–7.24 (m, 4H), 7.32–7.48 (m, 8H), 7.48–7.54 (m, 3H) ppm. ¹³C{¹H} NMR (CD₂Cl₂, 75 MHz): δ 134.9, 132.29, 131.6, 131.5, 129.3, 129.1, 128.9, 128.7, 65.8, 64.9, 56.1, 55.4, 49.8, 23.5 (observed 14 out of 15 expected signals). FTIR (KBr, cm⁻¹): 3061, 3032, 2931, 2872, 2358, 2074 (C≡O), 1499, 1456, 1348, 1204, 1072, 1038, 975, 916, 762, 743, 707, 657 (SbF₆). Anal. Calcd for CuN₃C₂₉H₃₅OSbF₆: C, 47.01; H, 4.76; N, 5.67. Found: C, 47.75; H, 4.94; N, 5.82.

[(iPr₃TACN)Cu(CH₃CN)]BPh₄. A solution of CuCl (0.20 g, 2.00 mmol) in CH₃CN (5 mL) was treated with a solution of iPr₃TACN (0.52 g, 2.04 mmol) in THF (3 mL). After stirring the colorless solution for 30 min, a solution of NaBPh₄ (0.68 g, 1.99 mmol) in CH₃CN (5 mL) was added, causing the precipitation of NaCl. After stirring for an additional 30 min the mixture was filtered through a pad of Celite and the filtrate treated with Et₂O (20 mL). Storage at -20 °C caused the deposition of colorless plate crystals of the product (1.09 g, 80%). ¹H NMR (500 MHz, CD₂Cl₂): δ 7.34–7.32 (m, 8H), 7.04 (t, *J* = 6.5 Hz, 8H), 6.89 (t, *J* = 7.5 Hz, 4H), 3.05 (heptet, *J* = 6.5 Hz, 3H), 2.79–2.72 (m, 6H), 2.48–2.42 (m, 6H), 1.94 (s, 3H), 1.20 (d, *J* = 6.5 Hz, 18H) ppm. ¹³C{¹H} NMR (125 MHz, CD₂Cl₂): δ 164.6, 135.4, 126.2, 126.1, 122.2, 58.6, 51.2, 20.0, 3.2 ppm. FTIR (KBr, cm⁻¹): 2265 (C≡N), 734 (BPh₄⁻), 704 (BPh₄⁻). Anal. Calcd for C₄₁H₅₆N₄BCu: C, 72.50; H, 8.31; N, 8.25. Found: C, 72.13; H, 8.33; N, 8.33.

Reactions of the Cu(I) Complexes with Dioxygen. Dry O₂ was bubbled through a precooled solution of [(iPr₃TACD)Cu(CH₃CN)]X (X = SbF₆⁻, ClO₄⁻, or BPh₄⁻) in CH₂Cl₂, acetone, or THF, [(Me₃TACD)Cu(CH₃CN)]X (X = SbF₆⁻, ClO₄⁻) in CH₂Cl₂ or THF, or [(Bn₃TACD)Cu(CH₃CN)]SbF₆ in CH₂Cl₂, THF, or acetone. The time required for full oxygenation, as indicated by maximization of the absorbance bands associated with the product(s), differed, with [(iPr₃TACD)Cu(CH₃CN)]X requiring 1 h of vigorous O₂ bubbling and [(Me₃TACD)Cu(CH₃CN)]X and [(Bn₃TACD)Cu(CH₃CN)]SbF₆ requiring only 5 min. Spectroscopic properties of the oxygenation products are listed in Table 3. The extinction coefficients of the UV-vis features were obtained from Beer's law plots (concentration ranges for the cases with iPr₃TACD = 0.16–0.60 mM; Me₃TACD = 0.04–0.17 mM; Bn₃TACD = 0.02–0.25 mM). Samples for resonance Raman spectroscopy were prepared by first dissolving the Cu(I) complex in the desired solvent (~5 mM) in a Schlenk flask. After cooling to -80 °C, dry O₂

was bubbled through the solution and a drop of the resulting colored solution was then quickly transferred via cold pipet onto a gold-plated copper coldfinger cooled to liquid N₂ temperature.

X-ray Crystallography. Crystals of [(iPr₃TACD)Cu(CH₃CN)]SbF₆, [(Me₃TACD)Cu(CH₃CN)]ClO₄, [(iPr₃TACDD)Cu]ClO₄, [(iPr₃TACD)₂-Cu₂(O₂)](BPh₄)₂, [(iPr₃TACD)₂Cu₂(CO₃)](BPh₄)₂, and [(Me₃TACD)₂Cu₂(OH)₂](ClO₄)₂ were attached to a glass fiber with epoxy and mounted on the Siemens SMART system for data collection. Initial sets of cell constants were calculated from reflections harvested from three sets of 20 frames oriented such that orthogonal wedges of reciprocal space were surveyed. Space groups were determined based on systematic absences and intensity statistics, and successful direct-methods solutions were calculated, which provided most non-hydrogen atoms. Several full-matrix least-squares/difference Fourier cycles were performed which located the remainder of the non-hydrogen atoms. All non-hydrogen atoms were refined with anisotropic displacement parameters unless stated otherwise. All hydrogen atoms were placed in ideal positions and refined as riding atoms with relative isotropic displacement parameters. The technique of hemisphere collection was used in which a randomly oriented region of reciprocal space was surveyed to the extent of 1.3 hemispheres to a resolution of 0.84 Å. Three major swaths of frames were collected with 0.30° steps in ω . The collection and refinement data are summarized in Table 2, and selected bond distances and angles are provided in the captions to Figures 1–4, 7, and 8. Complete descriptions of all structures, including full tables of positional parameters, interatomic distances and angles, and thermal parameters, are included in the Supporting Information. Crystallization methods and some unique attributes of each structure determination are as follows:

(a) [(iPr₃TACD)Cu(CH₃CN)]SbF₆. X-ray-quality crystals were obtained by slow diffusion of Et₂O into a solution of the complex in CH₃CN. The data were collected at 293(2) K due to an apparent phase change (as evidenced by observed shattering of the crystals) at low temperature. Orientation matrices were determined from 189 reflections, and the final cell constants were calculated from a set of 7194 strong reflections. The anisotropic displacement parameters of the iPr carbon atoms and those of the propyl group linking N(1) and N(2) were restrained to approximate rigid body motion.

(b) [(Me₃TACD)Cu(CH₃CN)]ClO₄. X-ray-quality crystals were obtained by slow diffusion of Et₂O into a solution of the complex in CH₃CN. The crystal was found to be rotationally twinned (0.87: 0.13); the structure is reported for the major twin only (twin law by rows 1 0 0, 0 -1 0, -1/3 0 -1).

(c) [(iPr₃TACDD)Cu]ClO₄. X-ray-quality crystals were obtained by slow diffusion of Et₂O into a solution of the complex in CH₂Cl₂.

(d) [(d₂₁-iPr₃TACD)₂Cu₂(μ - η^2 : η^2 -O₂)](BPh₄)₂. After numerous attempts to grow crystals of this complex using combinations of solvents (acetone, CH₂Cl₂, THF, 2-butanone, CH₃OH, and benzene) and counterions (ClO₄⁻, SbF₆⁻, and BPh₄⁻), the following procedure was found to be successful. Solid [(d₂₁-iPr₃TACD)Cu(CH₃CN)]BPh₄ (~0.14 g) was dissolved in CH₂Cl₂ (1 mL) and transferred into a crystallization tube. The solution of the Cu(I) complex was cooled to -80 °C, and O₂ was bubbled through the solution for 40 min. A precooled solution (1 mL) of acetone/2-butanone (1:1 v/v) was then carefully layered on top of the purple-red CH₂Cl₂ solution, and the resulting mixture was stored untouched at -80 °C for 6–10 days, leading to the deposition of purple-red rectangular-shaped crystals (sometimes mixed with green crystals, identified as the carbonate compound described in (e) below) that were carefully mounted so as to ensure no warming (which induced decomposition as indicated by conversion to green material). Orientation matrices were determined from 334 reflections, and the final cell constants were calculated from a set of 7729 strong reflections. All solvent in the structure was disordered, so PLATON/SQUEEZE²⁶ was used to remove the effect of the disordered solvent from the data in order to refine the remainder of the structure as accurately as possible.

The solution was possible in either *Pn* or *P2₁/n*; in the former a pair of iPr groups are ordered, but in the latter they must be disordered. This is the only significant obstacle to this structure being centrosymmetric. As a consequence, the two BPh₄⁻ anions and the monocopper

halves (including most of the iPr₃TACD ligand) are pseudosymmetrically related. The residuals for *Pn* are better than those for *P2₁/n* by ~3%, and the Hamilton test selects *Pn* as the better space group at the 99% confidence level. Still, many restraints were imposed to keep this fully anisotropically refined structure positive definite. The parts related by the pseudosymmetry were made to have similar σ and β bond distances by using the SAME restraint. Some groups had unreasonable thermal ellipsoids so DELU and SIMU restraints were applied where found necessary. Although the overall topology appears to be correct, the degree of precision implied by the small esds and low residuals should be viewed with skepticism, and we therefore refrain from analyzing interatomic distances and angles in detail.

(e) [(iPr₃TACD)₂Cu₂(CO₃)](BPh₄)₂. Green prisms of this complex cocrystallized with the (μ - η^2 : η^2 -peroxo)dicopper complex mentioned above. Orientation matrices were determined from 115 reflections, and the final cell constants were calculated from a set of 8192 strong reflections. Four solvent molecules of dichloromethane and 1.5 of acetone were located along with the two tetraphenylborates.

(f) [(Me₃TACD)₂Cu₂(OH)₂](ClO₄)₂. The oxygenation product [(Me₃TACD)₂Cu₂(O₂)](ClO₄)₂ in CH₂Cl₂ was warmed to room temperature. Slow evaporation of the resulting green solution at room temperature led to deposition of a few green crystals, which were mounted for data collection. Orientation matrices were determined from 40 reflections, and final cell constants were calculated from a set of 3699 strong reflections.

Computational Details. Calculations on [(L)₂Cu₂(O₂)]²⁺ (L = (NH₃)₃, TACN, and TACD) were performed with Gaussian94.²⁷ Calculations on the real systems [(L)₂Cu₂(O₂)]²⁺ (L = Me₃TACD or iPr₃TACD) were performed with the IMMOM program²⁸ built from modified versions of Gaussian92/DFT²⁹ and MM3(92).³⁰ In all cases, quantum mechanical calculations were carried out at the B3LYP level³¹ with basis sets LANL2DZ for Cu,³² 6-31G(d) for O,³³ and 6-31G for H, C, and N.³⁴ The MM3(92) force field³⁴ was used in the molecular mechanics part of the calculations. The van der Waals parameters for Cu were taken from the UFF force field³⁵ and torsional contributions involving dihedral angles with the metal atom in the terminal position were set to zero. All geometrical parameters were optimized except the bond distances connecting the QM and MM regions, which were kept constant: N–H (1.019 Å) and N–C (1.438 Å) in the QM and MM parts, respectively.

Acknowledgment. Financial support for this research was provided by the NIH (GM47365 to W.B.T., F32-GM19374 to J.R.H.), the NSF (National Young Investigator Award to

- (27) Frisch, M. J.; Trucks, G. W.; Schlegel, H. B.; Gill, P. M. W.; Johnson, B. G.; Robb, M. A.; Cheeseman, J. R.; Keith, T. A.; Petersson, G. A.; Montgomery, J. A.; Raghavachari, K.; Al-Laham, M. A.; Zakrzewski, V. G.; Ortiz, J. V.; Foresman, J. B.; Cioslowski, J.; Stefanov, B. B.; Nanayakkara, A.; Challacombe, M.; Peng, C. Y.; Ayala, P. Y.; Chen, W.; Wong, M. W.; Andres, J. L.; Replogle, E. S.; Gomperts, R.; Martin, R. L.; Fox, D. J.; Binkley, J. S.; Defrees, D. J.; Baker, J. P.; Stewart, J. P.; Head-Gordon, M.; Gonzalez, C.; Pople, J. A. *Gaussian 94*, revision C.3; Gaussian, Inc.: Pittsburgh, PA, 1995.
- (28) Maseras, F.; Morokuma, K. *J. Comput. Chem.* **1995**, *16*, 1170.
- (29) Frisch, M. J.; Trucks, G. W.; Schlegel, H. B.; Gill, P. M. W.; Johnson, B. G.; Wong, M. W.; Foresman, J. B.; Robb, M. A.; Head-Gordon, M.; Replogle, E. S.; Gomperts, R.; Andres, J. L.; Raghavachari, K.; Binkley, J. S.; Gonzalez, C.; Martin, R. L.; Fox, D. J.; Defrees, D. J.; Baker, J. P.; Stewart, J. P.; Pople, J. A. *Gaussian 92/DFT*; Gaussian, Inc.: Pittsburgh, PA, 1993.
- (30) Allinger, N. L., *MM3(92)*; QCPE: Bloomington, IN, 1992.
- (31) (a) Becke, A. D. *J. Chem. Phys.* **1993**, *98*, 5648. (b) Lee, C.; Yang, W.; Parr, R. G. *Phys. Rev. B* **1988**, *37*, 785. (c) Stephens, P. J.; Devlin, F. J.; Chabalowski, C. F.; Frisch, M. J. *J. Phys. Chem.* **1994**, *98*, 11623.
- (32) Hay, P. J.; Wadt, W. R. *J. Chem. Phys.* **1985**, *82*, 299.
- (33) (a) Hehre, W. J.; Ditchfield, R.; Pople, J. A. *J. Chem. Phys.* **1972**, *56*, 2257. (b) Hariharan, P. C.; Pople, J. A. *Theor. Chim. Acta* **1973**, *28*, 213.
- (34) (a) Allinger, N. L.; Yuh, Y. H.; Lii, J. H. *J. Am. Chem. Soc.* **1989**, *111*, 8551. (b) Lii, J. H.; Allinger, N. L. *J. Am. Chem. Soc.* **1989**, *111*, 8566. (c) Lii, J. H.; Allinger, N. L. *J. Am. Chem. Soc.* **1989**, *111*, 8576.
- (35) Rappé, A. K.; Casewit, C. J.; Cowell, K. S.; Goddard, W. A., III.; Skiff, W. M. *J. Am. Chem. Soc.* **1992**, *114*, 10024.

W.B.T.), the Camille and Henry Dreyfus and Alfred P. Sloan Foundations (fellowships to W.B.T.), and the Direcció General de Ensenanza Superior e Investigaci6n Científica (DGESIC, Grants PB98-1166-C02-01 and PB98-0916-CO2-01 to S.A. and A.L.). Allocation of computer time at the Centre de Supercomputaci6 de Catalunya (CESCA) was in part funded through grants from the Fundaci6 Catalana per a la Recerca (FCR), Comissió Interdepartamental de Recerca i Innovaci6 Tecnol6gica (CIRIT), and the Universitat de Barcelona. The authors thank F. Maseras for invaluable technical advice on IMOMM calculations.

Supporting Information Available: ^1H – ^1H COSY spectrum of $[(i\text{Pr}_3\text{TACD})\text{Cu}(\text{CH}_3\text{CN})]^+$ (Figure S1), structural comparisons and ligand conformational analyses of Cu(I) complexes (Figures S2 and S3), cyclic voltammograms (Figure S4), spectroscopic and kinetic data for oxygenated complexes (Figures S5–S8), plot of calculated Cu–N distances as a function of the orientation of the Cu–N bond in TACD-supported Cu_2O_2 compounds (Figure S9), and full X-ray crystallographic data including tables of bond lengths and angles and thermal parameters. This material is available free of charge via the Internet at <http://pubs.acs.org>.

IC000248P